PHILOSOPHICAL TRANSACTIONS OF THE ROYAL SOCIETY B BIOLOGICAL SCIENCES

A Model for Rebound Bursting in Mammalian Neurons

J. L. Hindmarsh and R. M. Rose

Phil. Trans. R. Soc. Lond. B 1994 **346**, 129-150
doi: 10.1098/rstb.1994.0137

A model for rebound bursting in mammalian neurons

J. L. HINDMARSH[1] AND R. M. ROSE[2]

School of Mathematics[1] and Department of Physiology[2], University of Wales College of Cardiff, Cathays Park, Cardiff CF1 1SS, U.K.

SUMMARY

In this paper we begin by simplifying our previous model of a thalamic neuron (Rose & Hindmarsh *Proc. R. Soc. Lond.* B **237**, 289–312 (1989*b*)) by removal of the A current. A Ca^{2+}-activated K^+ current, with Ca^{2+} entering through T channels, is then added to give a model for a class of mammalian neurons in which the membrane potential oscillates in the subthreshold region following a hyperpolarizing current step. The properties of the model are represented using an experimentally observable bifurcation diagram. In the subthreshold region only three variables are required to explain the essential dynamic properties of the cell. In this three-dimensional space the solutions tend to lie on a surface which resembles a paraboloid. We use a simplified model of this model to explain both the dynamics of the solutions on this surface and the form of the bifurcation diagram.

1. INTRODUCTION

We have previously discussed a model of a thalamic neuron (Rose & Hindmarsh 1989*a–c*) which explained many of the experimental observations that Jahnsen & Llinás (1984*a*,*b*) made on thalamic cells. These cells had the property that a depolarizing current step, of fixed magnitude and duration, applied to the cell in steadily hyperpolarized equilibrium, at rest and in steadily depolarized equilibrium, produced three distinct effects.

1. When hyperpolarized the cell responded with a low threshold spike (LTS) whose peak exceeded threshold to give a burst of action potentials.

2. When at rest the response was a passive depolarization.

3. When depolarized the cell fired action potentials repetitively (tonic firing).

In addition:

4. If the cell was hyperpolarized from rest by a current step of sufficient magnitude and duration, it responded with a single rebound burst on termination of the step.

5. For a range of externally applied currents the cell may generate a periodic LTS.

Our model explained these properties. In particular the burst response was explained by the presence of a low threshold transient inward Ca^{2+} current which was deinactivated by hyperpolarization. The existence of this T-type current in thalamic neurons was later confirmed by voltage clamp experiments (Coulter *et al.* 1989; Crunelli *et al.* 1989; Hernandez-Cruz & Pape 1989).

Since that time thalamic neurons have been shown to have other ionic currents such as a fast and a slow A-current (Huguenard *et al.* 1991; Huguenard & Prince 1991) and a hyperpolarization activated cation current (McCormick & Pape 1990). These ionic currents contribute in different ways to the shape of the LTS and the form of the pacemaker cycle when the cell is oscillating. The simultaneous presence of the five properties listed above does not depend on them. Simulation models incorporating these and other ionic currents and with improved descriptions of I_T have been given by Wang *et al.* (1991), McCormick & Huguenard (1992), Toth & Crunelli (1992), Lytton & Sejnowski (1992), Wang (1994) and Destexhe & Babloyantz (1993). The discovery of the precise roles of each of these currents is important for the understanding of the physiology of the cells because they determine the frequencies of burst and tonic firing. However, with the exception of intrinsic spindle generation (Soltez *et al.* 1991; Destexhe & Babloyantz 1993; Destexhe *et al.* 1993) the role of these additional currents appears to be quantitative rather than to produce a qualitative change in the dynamics of the cell (McCormick & Huguenard 1992).

In this paper we extend our previous model to a class of neurons which are similar to thalamic neurons but show more complicated rebound responses. These include cells of the lateral habenula (LHb) nucleus (Wilcox *et al.* 1988), the nucleus reticularis thalami (nRT) (Avanzini *et al.* 1989; Bal & McCormick 1993) and the inferior olivary (IO) nucleus (Llinás & Yarom 1986; Yarom 1991). A typical example is given by LHb neurons which rebound with three or four bursts whose amplitude decays as the membrane potential returns to rest. The cell may also rebound to give continuous bursting. Inferior olivary cells give similar decaying oscillations in the presence of harmaline and tetrodotoxin (TTX) (Gutnick & Yarom 1989; Yarom 1991). In the case of nRT cells

Phil. Trans. R. Soc. Lond. B (1994) **346,** 129–150
Printed in Great Britain

the rebound bursts are frequently followed by a period of tonic firing (Bal & McCormick 1993).

In this paper we show that such rebound oscillations can be produced by the addition of a Ca^{2+}-activated K^+ current to our previous thalamic model (Rose & Hindmarsh 1989*b*,*c*). We assume that the Ca^{2+} ions enter through T channels, and refer to this K^+ current as $I_{KCa(T)}$. Assuming that the T channels are located in the somatic membrane and that Ca^{2+} ions diffuse slowly in the cytoplasm (Llinás 1988), it should be possible to test for the presence of $I_{KCa(T)}$ using the voltage clamp technique (see § 11). As shown below the addition of $I_{KCa(T)}$ produces a change in the bifurcation diagram and thus a qualitative change in the dynamics of the cell.

The idea that rebound oscillations might result from the interaction of I_T and one or more Ca^{2+}-activated K^+ currents has been suggested by the authors of the papers on LHb, nRT and IO neurons and has appeared in several preliminary models of nRT neurons (Wang & Rinzel 1993; Destexhe *et al.* 1993). Also the presence of these currents has been largely confirmed in the case of nRT neurons (Avanzini *et al.* 1989; Bal & McCormick 1993). However, our purpose is not simply to report the effect of adding $I_{KCa(T)}$ but to gain some understanding of the mechanism underlying these oscillations by taking the analysis of the differential equations further than in our previous work (Rose & Hindmarsh 1989*a*–*c*).

The mathematical sections of the paper may be summarized as follows. Numerical integration of the three-dimensional system of equations (4) describing this physiological model showed that in addition to a stable equilibrium point (EP), at the resting potential, the system had both a stable and an unstable limit cycle. To understand how this physiological model works we developed a simplified model, or 'model of the model'. The purpose of this was to give a simple explanation of how the stable and unstable limit cycles appear, how their location changes for different external currents and how the system responds to time varying external currents. In the following paper (Hindmarsh & Rose 1994*a*) we will show that the physiological model has the property that for a range of external currents the cell resonates to inputs at certain frequencies. The advantage of developing the model of the model in this paper is that it enables us to investigate this resonant behaviour analytically. In fact without the preliminary analysis of this paper we would have been unaware of the possibility of resonance in cells of this type (Hindmarsh & Rose 1994*a*) and of its possible physiological significance (Hindmarsh & Rose 1994*b*).

A preliminary report of the models discussed in this paper has already been given (Hindmarsh & Rose 1992).

2. THE SIMPLIFIED THALAMIC MODEL

In Rose & Hindmarsh (1989*a*–*c*) we started from the Hodgkin–Huxley equations (Hodgkin & Huxley 1952) and the equations of Connor & Stevens (1971) describing a fast transient outward current I_A. To these we added a further equation for the low threshold transient calcium current I_T described in the Introduction. The equations for this seven-dimensional system are:

$$\left.\begin{aligned}
\dot{v} &= C^{-1}\{-I_{Na} - I_K - I_L - I_A - I_T + I_{Ext}\},\\
\dot{m} &= \tau_m^{-1}(v)(m_\infty(v) - m),\\
\dot{h} &= \tau_h^{-1}(v)(h_\infty(v) - h),\\
\dot{n} &= \tau_n^{-1}(v)(n_\infty(v) - n),\\
\dot{a} &= \tau_a^{-1}(v)(a_\infty(v) - a),\\
\dot{b} &= \tau_b^{-1}(v)(b_\infty(v) - b),\\
\dot{h}_T &= \tau_{h_T}^{-1}(v)(h_{T_\infty}(v) - h_T),
\end{aligned}\right\} \quad (1)$$

where $I_{Na} = g_{Na}m^3h(v - v_{Na})$, $I_K = g_Kn^4(v - v_K)$, $I_A = g_Aa^3b(v - v_K)$, $I_T = g_T m_{T_\infty}(v)h_T(v - v_{Ca})$, and $I_L = g_L(v - v_L)$. Further details of these equations may be seen in Rose & Hindmarsh (1989*a*–*c*) where, it should be noted, we used the terms I_{s_a}, g_{s_a}, $s_{a_\infty}(v)$, h_a, τ_{h_a} and I instead of I_T, g_T, $m_{T_\infty}(v)$, h_T, τ_{h_T} and I_{Ext} used here.

Our present interest is in the behaviour of the cell in the subthreshold region. In this region the membrane potential changes slowly and various approximations are possible. For instance Wang *et al.* (1991) put $g_A = g_K = g_{Na} = 0$, replacing I_{Na}, I_K, and I_A by an 'effective' leakage current. We first discard the A-current, I_A, to obtain the five dimensional system:

$$\left.\begin{aligned}
\dot{v} &= C^{-1}\{-I_{Na} - I_K - I_L - I_T\\
&\qquad + I_0 + I + I(t)\},\\
\dot{m} &= \tau_m^{-1}(v)(m_\infty(v) - m),\\
\dot{h} &= \tau_h^{-1}(v)(h_\infty(v) - h),\\
\dot{n} &= \tau_n^{-1}(v)(n_\infty(v) - n),\\
\dot{h}_T &= \tau_{h_T}^{-1}(v)(h_{T_\infty}(v) - h_T).
\end{aligned}\right\} \quad (2)$$

Here we have written the external current, I_{Ext}, in the form $I_{Ext} = I_0 + I + I(t)$ where by definition I_0 has the value $-1.35\,\mu A\,cm^{-2}$ throughout, I is an additional constant current and $I(t)$ a time varying applied current such as a pulse, step or periodic current. The reason for introducing I_0 will be given in § 7.

Typical voltage responses obtained by numerical integration of equations (2) for a fixed amplitude step, $I(t)$, at various levels of steadily applied current, $I_0 + I$, are shown in figure 1*d*–*f*. Parameter values for these equations are given in Appendix 1.

We now remove the sodium current, I_{Na}, by putting $g_{Na} = 0$. The voltage-dependent K^+ current I_K is retained, because this allows us to add fast action potentials by reintroducing I_{Na}. We also find that I_K plays a significant role in repolarization of the low threshold oscillations in the model described below. Because I_K is small in the subthreshold region we do

PHILOSOPHICAL TRANSACTIONS OF THE ROYAL SOCIETY B BIOLOGICAL SCIENCES

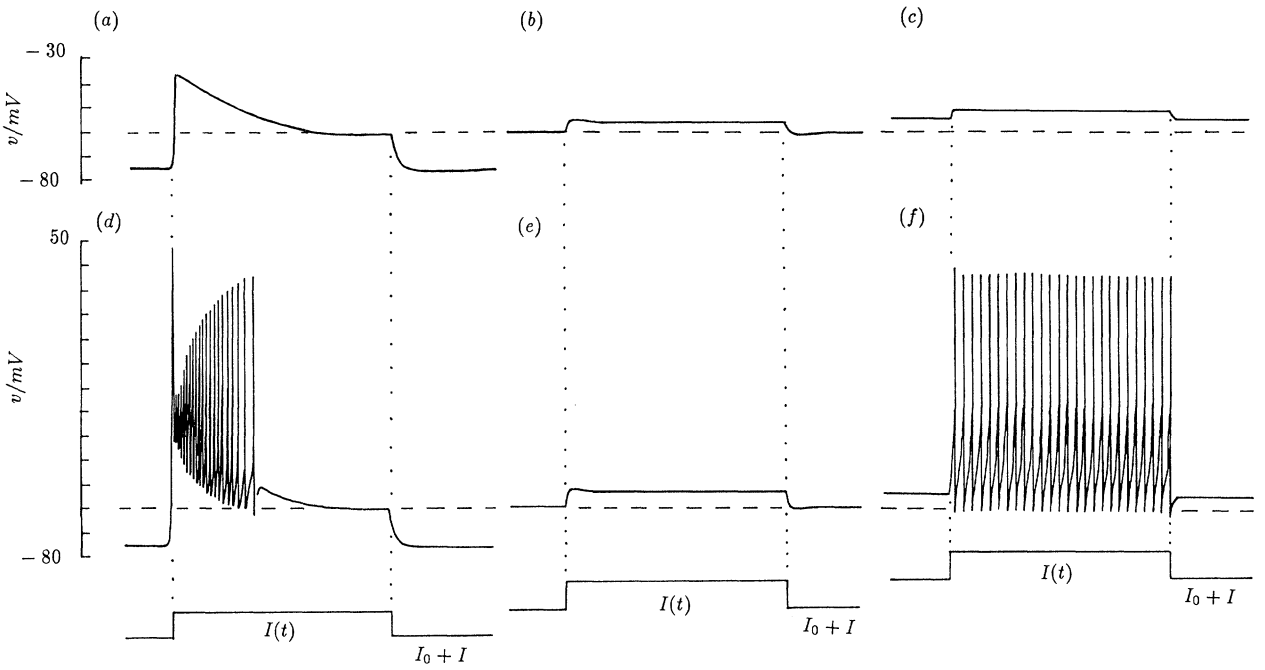

Figure 1. (*a*)–(*c*) Responses of the two-dimensional thalamic model (equations (3)) to current steps, $I(t)$, of amplitude $4.12\,\mu A\,cm^{-2}$ and 150 ms duration, at different levels of steady external current $I_0 + I = -4.12\,\mu A\,cm^{-2}$ (*a*), $0\,\mu A\,cm^{-2}$ (*b*) and $4.12\,\mu A\,cm^{-2}$ (*c*). (*d*)–(*f*) Responses of the five-dimensional thalamic model (equations (2)) to current steps, $I(t)$, of the same amplitude and duration, and with the same steady external currents, $I_0 + I$, as in (*a*–*c*). All figures obtained by numerical integration with the other parameter values given in Appendix 1.

however make the approximation $n \approx n_\infty(v)$. This leaves us with two equations:

$$\left.\begin{aligned} \dot{v} &= C^{-1}\{-g_L(v - v_L) - g_K n_\infty^4(v)(v - v_K) \\ &\quad - g_T m_{T_\infty}(v) h_T (v - v_{Ca}) + I_0 + I + I(t)\}, \\ \dot{h}_T &= \tau_{h_T}^{-1}(h_{T_\infty}(v) - h_T). \end{aligned}\right\} \quad (3)$$

In figure 1*a*–*c* we show voltage responses of equations (3) to the same sequence of current steps as shown for the five-dimensional model in figure 1*d*–*f*. The parameter values, given in Appendix 1, were chosen so that a limit cycle is present for a range of values of $I_0 + I$. As the external current is varied, the voltage coordinate of the resting equilibrium point (EP) changes as does the amplitude of the stable limit cycle. These changes are shown in the bifurcation diagram of figure 2*a*, where for each value of the external current, $I_0 + I$, represented on the horizontal axis, is shown the membrane potential of the EP and the maximum and minimum values of the membrane potential around a limit cycle if present. An interesting feature of this diagram is that as the external current becomes increasingly negative from the bifurcation point the amplitude of the limit cycle grows slowly at first, where the oscillations are almost sinusoidal (figure 2*b*), then rapidly to give large amplitude oscillations (figure 2*c*). The reason for this is the large distortion of the v nullcline, in the region $v \approx -73$ mV, which occurs with decreasing external current as shown in figure 2*d*,*e*. This is due to the comparative smallness of $m_{T_\infty}(v)$ in this region. This transition from small amplitude oscillations to larger oscillations as the cell is progressively hyperpolarized has been observed in thalamic neurons (Leresche *et al.* 1991, figure 2).

These results confirm that it is possible to replace our earlier three-dimensional (Rose & Hindmarsh 1989*b*) and seven-dimensional (Rose & Hindmarsh 1989*c*) models by simpler two- and five-dimensional models.

3. THE PHYSIOLOGICAL MODEL FOR REBOUND BURSTING

To explain the low threshold oscillations of lateral habenula and other cells we will add a further current to equations (3). To understand how this current will modify the behaviour of equations (3) we examine the nullclines of these equations for various values of constant external current $I_0 + I$. Figure 3*a*–*d* shows these nullclines for $I_0 + I = 0$, -3.4, -3.7 and $-4.12\,\mu A\,cm^{-2}$ (these values, particularly the latter, were chosen for illustrative purposes).

In the model described by equations (3), suppose the system is initially at rest in the equilibrium point A of figure 3*a*. If the system is hyperpolarized using a negative step $I(t) = -4.12\,\mu A\,cm^{-2}$ for 100 ms, then the state of the system will change to the equilibrium point B of figure 3*d*. On release of the step the state of the system returns to the original resting equilibrium point, without oscillation, as indicated in figure 3*a*. Using the full equations (2) this return would initiate the firing of just one rebound burst.

To generate a decaying succession of bursts, we want a low threshold damped oscillatory return to the resting equilibrium point. This oscillation would occur if, as a result of both the hyperpolarization and subsequent release, an outward current were activated that would leave the system as though subject to a

PHILOSOPHICAL TRANSACTIONS OF THE ROYAL SOCIETY B BIOLOGICAL SCIENCES

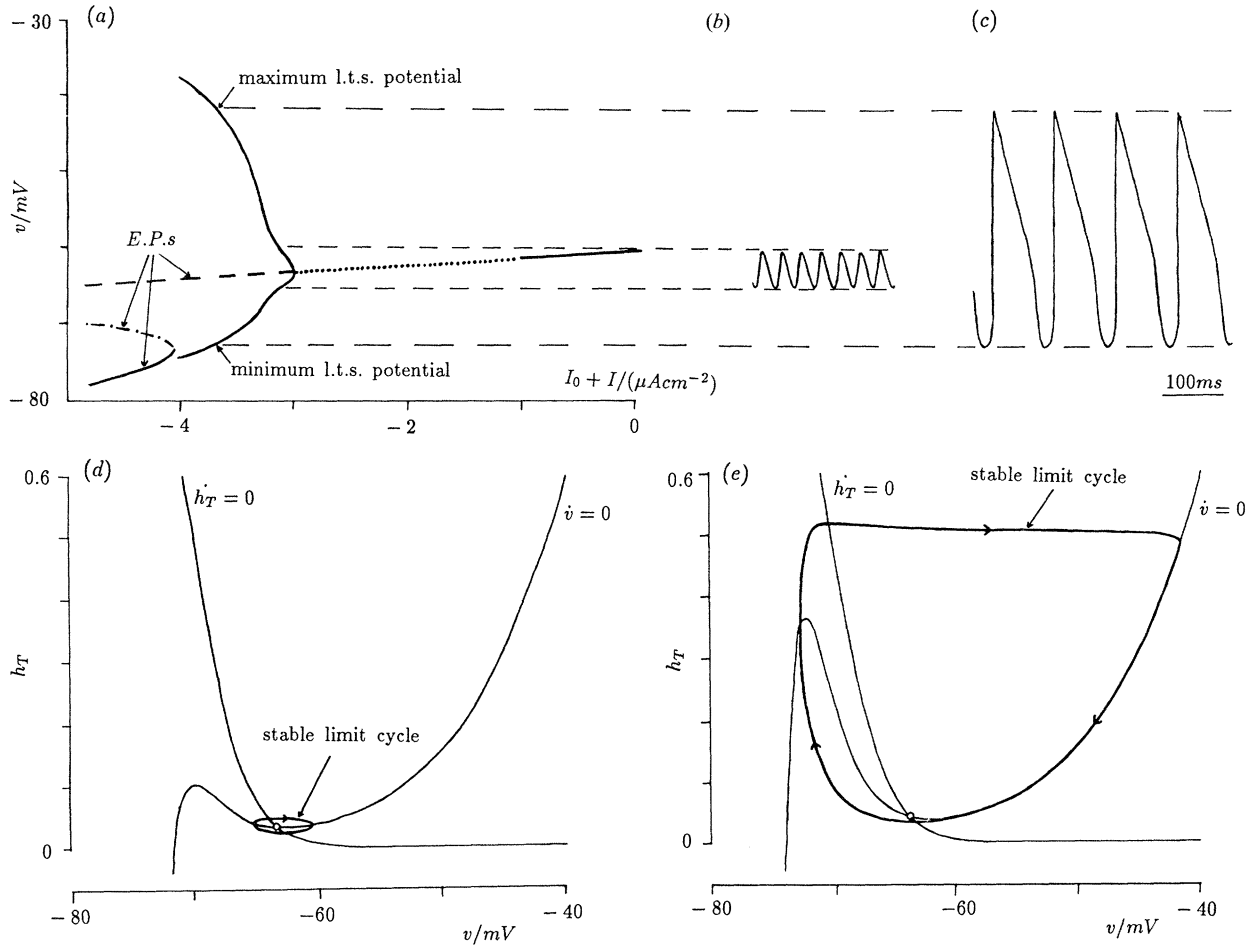

Figure 2. (*a*) $(I_0 + I, v)$ bifurcation diagram of the two-dimensional simplified thalamic model (equations (3)). Sloping line and curves on the lower left give voltage coordinates of EPs at different values of $I_0 + I$. Stability of these EPs is indicated as follows: long-dashed line, stable node; dotted line, stable spiral; short-dashed line, unstable node or spiral; dot-dashed line, unstable saddle. Amplitudes of limit cycle solutions between $I_0 + I \approx -3\,\mu A\,cm^{-2}$ and $I_0 + I \approx -4\,\mu A\,cm^{-2}$ are indicated by the two solid curves leaving the line of EPs at $I_0 + I \approx -3\,\mu A\,cm^{-2}$. (*b*) Small amplitude, and (*c*) large amplitude limit cycle solutions of equations (3) with $I_0 + I = -3.12\,\mu A\,cm^{-2}$ and $-3.7\,\mu A\,cm^{-2}$ respectively. Horizontal dashed lines connect maximum and minimum values of membrane potential with corresponding pairs of points on the bifurcation diagram. (*d*) (v, h_T) nullcline diagram and limit cycle for the small amplitude limit cycle shown in (*b*). (*e*) (v, h_T) nullcline diagram and limit cycle for the large amplitude limit cycle shown in (*c*). Other parameter values given in Appendix 1.

constant external current of, say, $-3.7\,\mu A\,cm^{-2}$. The nullclines would then be as in figure 3*c* and the state of the system would follow the limit cycle path. In reality the outward current need not be constant. If it decayed then the oscillations would decrease in amplitude (figure 3*b*) and the system would return to the resting equilibrium point.

This outward current could be either voltage-dependent or Ca^{2+}-dependent. We will consider a Ca^{2+}-activated K^+ current and comment afterwards on an alternative.

The Ca^{2+}-activated K^+ current is given by:

$$I_{KCa(T)} = g_{KCa(T)}\left(\frac{c}{K_{Ca(T)} + c}\right)(v - v_K),$$

where $g_{KCa(T)}$ and $K_{Ca(T)}$ are conductivity and dissociation constants respectively and c measures the concentration of intracellular free calcium (for similar models, see Plant 1978; Chay & Keizer 1983; Rinzel & Lee 1986). The differential equation for c is:

$$\dot{c} = -kI_T - k_{Ca}c \quad (= -kg_T m_{T_\infty}(v)h_T(v - v_{Ca}) - k_{Ca}c),$$

where k and k_{Ca} are constants whose values will be chosen following the discussion below. Later in § 11 we will explain how these values can be obtained from voltage clamp experiments.

This gives the following three-dimensional system:

$$\left.\begin{aligned} \dot{v} &= C^{-1}\{-g_L(v - v_L) - g_K n_\infty^4(v)(v - v_K) \\ &\quad - g_T m_{T_\infty}(v)h_T(v - v_{Ca}) \\ &\quad - g_{KCa(T)}\left(\frac{c}{K_{Ca(T)} + c}\right)(v - v_K) \\ &\quad + I_0 + I + I(t)\}, \\ \dot{h}_T &= \tau_{h_T}^{-1}(h_{T_\infty}(v) - h_T), \\ \dot{c} &= -kg_T m_{T_\infty}(v)h_T(v - v_{Ca}) - k_{Ca}c. \end{aligned}\right\} \quad (4)$$

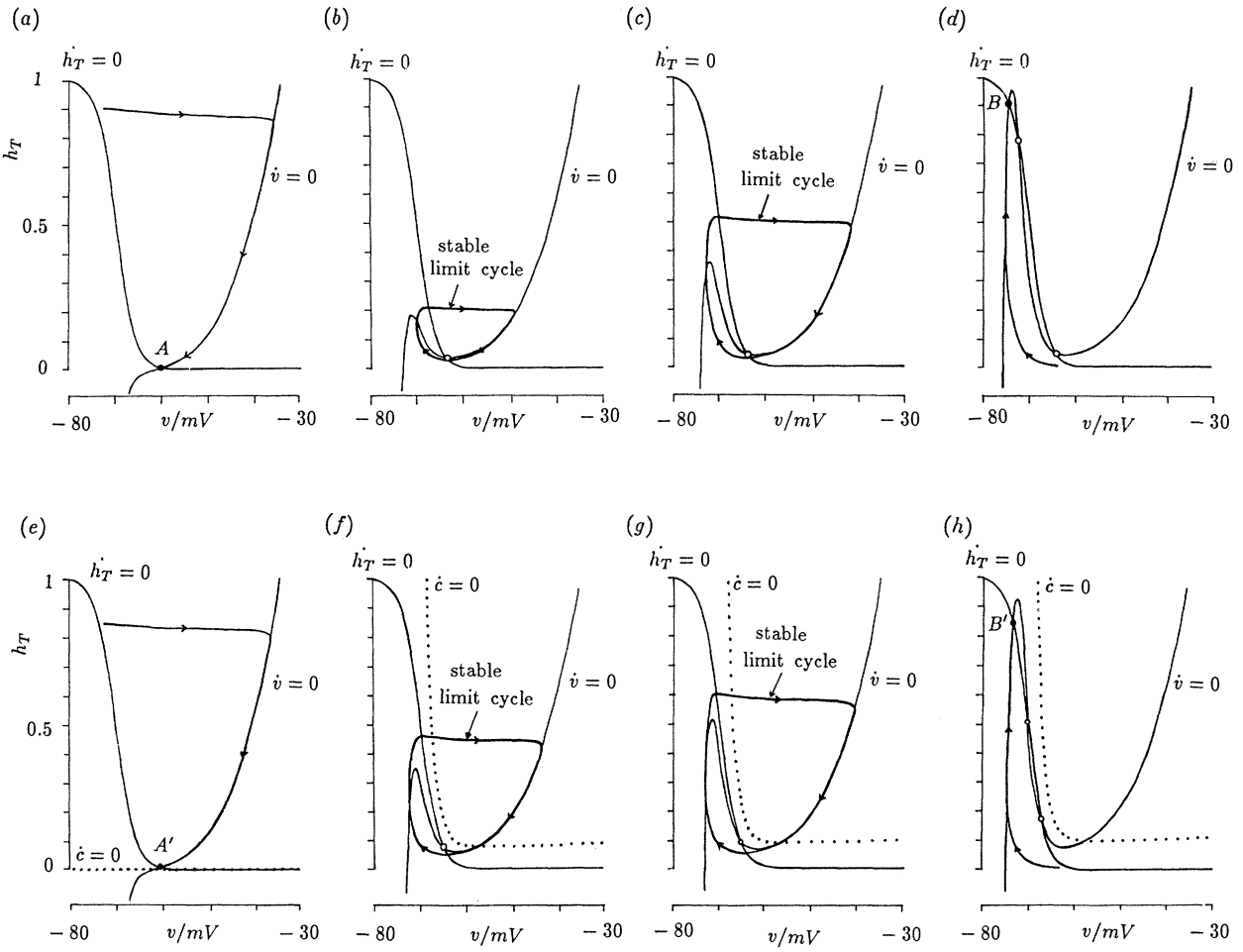

Figure 3. (*a*)–(*d*) (v, h_T) nullcline diagrams for the simplified thalamic model (equations (3)) for $I_0 + I = 0\,\mu A\,cm^{-2}$ (*a*), $-3.4\,\mu A\,cm^{-2}$ (*b*), $-3.7\,\mu A\,cm^{-2}$ (*c*), and $-4.12\,\mu A\,cm^{-2}$ (*d*). (*e*)–(*h*) (v, h_T) nullcline diagrams for the first two of equations (4) with $c = c_0 = 0\,\mu M$ (*e*), $0.20\,\mu M$ (*f*), $0.22\,\mu M$ (*g*) and $0.25\,\mu M$ (*h*). Other parameter values given in Appendix 1. See text for further explanation.

In choosing parameter values for $I_{KCa(T)}$ we assume that $K_{Ca(T)} = 1\,\mu M$ (see Chay & Keiser 1983) and that $g_{KCa(T)} = 2g_T = 1.2\,mS\,cm^{-2}$. The effect on the bifurcation diagram, of varying $g_{KCa(T)}$, will be discussed in § 6.

If we take the first two of equations (4) and give c the constant value c_0 then we obtain a system similar to that described by equations (3). Equations (3) have a limit cycle solution when $I_0 + I = -3.7\,\mu A\,cm^{-2}$ as shown in figure 3*c*. The first two of equations (4) would have a similar limit cycle with $I_0 + I = 0$ provided that we could choose c_0 so that $I_{KCa(T)} = -3.7\,\mu A\,cm^{-2}$. This cannot be done exactly as $I_{KCa(T)}$ is voltage dependent through the term $(v - v_K)$. We can see from figure 3*a*–*d* that the change in the configuration of the v nullcline with $I_0 + I$ is most marked when $v \approx -73\,mV$. Thus we choose c_0 so that $I_{KCa(T)}$ has the value $-3.7\,\mu A\,cm^{-2}$ when $v = -73\,mV$. This means that c_0 is given by:

$$-g_{KCa(T)}\left(\frac{c_0}{K_{Ca(T)} + c_0}\right)(-73 - v_K) = -3.7,$$

which gives $c_0 = 0.22\,\mu M$.

With this value for c_0 the first two of equations (4) have nullclines and limit cycle as shown in figure 3*g*. Similarly figure 3*e*,*f*,*h* show the nullclines for the first two of equations (4) with $c_0 = 0$, 0.2, and $0.253\,\mu M$ respectively. Note that these are not exactly the same as figure 3*a*–*d* because of the voltage dependence of $I_{KCa(T)}$. The dotted curves in figure 3*e*–*h* will be referred to in the next section.

We now consider the effect of the third of equations (4). In particular we wish to see how one might choose parameters in this equation so that it allows the system to oscillate following a hyperpolarizing step. With c_0 fixed at $0.22\,\mu M$ the average value $\langle I_T \rangle$ of I_T can be estimated from the limit cycle solution of the first two of equations (4). We now arrange that the effect of the third of equations (4) is to give c an average value of $0.22\,\mu M$. This requires that:

$$\frac{-k\langle I_T \rangle}{k_{Ca}} = 0.22\,\mu M.$$

By choosing a value for k to give a time constant of decay of low threshold oscillations similar to that of the real cell, this equation gives a value for k_{Ca}. Although this value for k_{Ca} does give the desired low threshold oscillation, following a hyperpolarizing pulse, we decreased the value for reasons to be given in § 6.

An alternative to the above model could be developed using a voltage-dependent outward current. In the case of a voltage-dependent K^+ current there are several possible combinations of activation and inactivation variables that could be used. Our investigations of these models suggest that the best model of this type is:

$$\left.\begin{aligned} \dot{v} &= C^{-1}\{-I_{\mathrm{L}} - I_{\mathrm{K}} - I_{\mathrm{T}} - g_z z(v - v_{\mathrm{K}}) \\ &\quad + I_0 + I + I(t)\}, \\ \dot{h}_{\mathrm{T}} &= \tau_{h_{\mathrm{T}}}^{-1}(h_{\mathrm{T}_\infty}(v) - h_{\mathrm{T}}), \\ \dot{z} &= \tau_z^{-1}(z_\infty(v) - z), \end{aligned}\right\} \qquad (5)$$

where

$$z_\infty(v) = \frac{1}{1 + \exp(-\gamma_z(v - \theta_z))}, \quad \gamma_z > 0, \quad \theta_z < 0.$$

Although these equations can give rebound oscillations to a negative current step, the z variable is also activated by a positive current step unless strict conditions are imposed on the definition of z_∞ (see Rose & Hindmarsh 1989*a*). This means that on termination of a positive current step the system will also tend to oscillate. Experimentally, depolarizing current steps applied, for instance, to LHb neurons result in tonic firing which is not followed by oscillations on termination of the step (Wilcox *et al.* 1988). As shown above our solution to this problem was to use a Ca^{2+}-activated K^+ current $I_{\mathrm{KCa(T)}}$. This current is dependent on the entry of T-channel Ca^{2+}, and so positive current steps, applied to the cell at rest, will not activate $I_{\mathrm{KCa(T)}}$ because I_{T} is largely inactivated at rest. Consequently we are able to obtain rebound oscillations for negative current steps and the required form of tonic firing for positive current steps.

A further justification for investigating the effect of adding $I_{\mathrm{KCa(T)}}$ to equations (3) comes from the experimental results of Avanzini *et al.* (1989) and Bal & McCormick (1993). They have shown that in rat nRT neurons Ca^{2+} entry during the LTS activates a fast and a slow apamin-sensitive Ca^{2+}-dependent K^+ current. These outward currents cause a deep after-hyperpolarization in nRT neurons, whose electrophysiological properties are very similar to those of LHb neurons. Apamin-sensitive K^+ currents are known to be strongly dependent on intracellular Ca^{2+} (Blatz & Magleby 1987).

4. THE STATE SPACE OF THE PHYSIOLOGICAL MODEL

Numerical integration of equations (4) with the parameter values given in Appendix 1 and with $I_0 + I = 0$ show that the solutions are attracted to a surface whose shape approximates that of a paraboloid (see figure 4*a*). On this paraboloid there is a

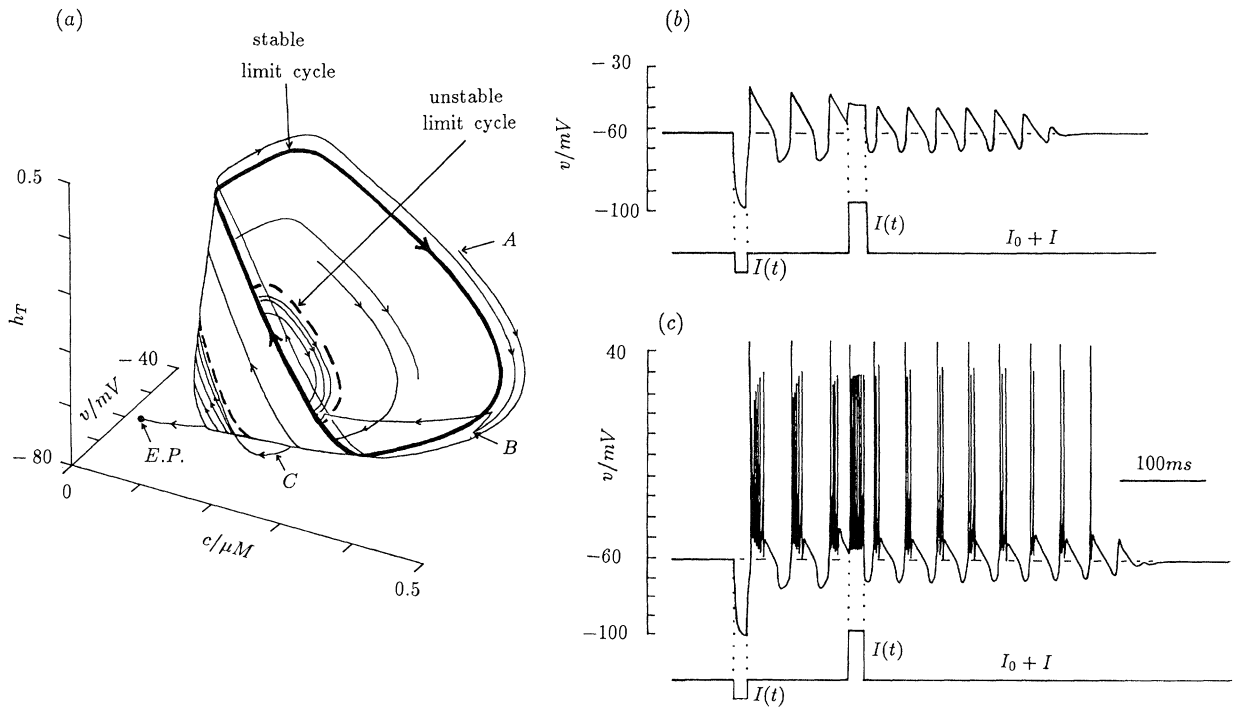

Figure 4. (*a*) Attractor surface for standard three-dimensional physiological model (equations (4)) with $I_0 + I = 0\,\mu\mathrm{A\,cm^{-2}}$, showing stable and unstable limit cycles. Also shown is state path for numerical solution shown in (*b*). Note that a depolarizing current step applied at point B displaces the state to point C just below the unstable limit cycle. (*b*) Numerical solution of equations (4) with $I_0 + I = 0\,\mu\mathrm{A\,cm^{-2}}$ to a hyperpolarizing current step, $I(t)$, of amplitude $-10\,\mu\mathrm{A\,cm^{-2}}$ and 20 ms in duration, followed by a depolarizing current step of amplitude $25\,\mu\mathrm{A\,cm^{-2}}$ and 28.5 ms in duration. The time interval between the onset of the hyperpolarizing current step and the onset of the depolarizing current step was 185 ms. (*c*) Numerical solution of the six dimensional physiological model (equations (6)) for the same external current and current steps as in (*b*). Other parameter values given in Appendix 1.

stable limit cycle and an unstable limit cycle. Near its vertex the solutions leave the surface and approach the stable EP.

This surface appears because if the first two of equations (4) are integrated, with c given a constant value c_0 and $I_0 + I = 0$, we find, for small values of c_0, a stable EP and, for larger values of c_0, a stable limit cycle as shown in figure 3*e–h*. When all three equations are integrated the value of c changes and the solution does not lie in a plane of constant c_0 (see for instance the limit cycles shown in figure 4*a*). If we look at a plane $c = c_0$ in the state space, we can divide it into regions where $\dot{c} < 0$ and where $\dot{c} > 0$ by the points where $\dot{c} = 0$, that is the curve:

$$-kI_T - k_{Ca}c_0 = 0,$$

or equivalently:

$$-kg_T m_{T_\infty}(v)h_T(v - v_{Ca}) - k_{Ca}c_0 = 0.$$

These points are shown by dotted curves in figure 3*e–h*. They are the intersections of the c nullsurface with the planes of constant c.

As a solution goes around the paraboloid the value of c will increase and decrease. After one circuit a net decrease in the value of c will be reflected in a movement towards the vertex and vice versa.

An interesting test of this model is shown in figure 4*b*. Here a hyperpolarizing current step is applied to give rebound into bursting that would be continuous if no further current steps were applied. In this example a depolarizing current step was applied late in the positive phase of the third cycle. The evolution of the system as a result of these steps is shown in figure 4*a*. On release of the hyperpolarizing step the state of the system is on the paraboloid just above the stable limit cycle. During the next three oscillations the state winds down the paraboloid towards the stable limit cycle. In figure 4*a* we show the state path beginning at a point A on the third cycle. When the system is at the point B shown in figure 4*a*, the depolarizing step displaces the state to a point C just below the unstable limit cycle. It then winds around the paraboloid a few more times before drifting off to the stable resting EP. The corresponding time course of the membrane potential is shown in figure 4*b*. Note that after the depolarizing current step the oscillations are of a smaller amplitude and a higher frequency than the initial rebound oscillations. This experiment has been carried out by Wilcox *et al.* (1988) and is shown in figure 14 of their paper. To compare our model with their recording we return to the complete system of six differential equations:

$$\left.\begin{aligned}
\dot{v} &= C^{-1}\{-I_{Na} - I_K - I_L - I_T - I_{KCa(T)} \\
&\quad + I_0 + I + I(t)\}, \\
\dot{m} &= \tau_m^{-1}(v)(m_\infty(v) - m), \\
\dot{h} &= \tau_h^{-1}(v)(h_\infty(v) - h), \\
\dot{n} &= \tau_n^{-1}(v)(n_\infty(v) - n), \\
\dot{h}_T &= \tau_T^{-1}(h_{T_\infty}(v) - h_T), \\
\dot{c} &= -kg_T m_{T_\infty}(v)h_T(v - v_{Ca}) - k_{Ca}c.
\end{aligned}\right\} \quad (6)$$

As shown in figure 4*b,c* the main difference between the solution of the reduced system of equations (figure 4*b*) and the corresponding solution of the full system of equations (figure 4*c*) is the appearance of the action potentials in the latter. This solution of the full system compares well with the experimental recording of Wilcox *et al.* (1988). Given the complexity of this experimental recording it would seem that the model has captured the main features of the dynamical system underlying the behaviour of the cell. We will, however, suggest an improvement in § 6, based on the voltage separation of the half activation points for m_{T_∞} and h_{T_∞}, following the discussion of the bifurcation diagram.

5. THE BIFURCATION OF THE PHYSIOLOGICAL MODEL

Figure 5*a* is a bifurcation diagram for the three-dimensional system (equations (4)) with the parameter values given in Appendix 1. This diagram should be compared with figure 2*a* because the parameter values for I_L, I_K, and I_T are the same in both cases. The only difference is that $I_{KCa(T)}$ is present in figure 5*a* and absent in figure 2*a*. The effect of introducing $I_{KCa(T)}$ is as follows. For $I < I_1$ there is a stable EP. For $I_1 < I < I_2$ there is an unstable EP, whose membrane potential is shown with a dashed line, and a stable limit cycle. For $I_2 < I < I_3$ there is a stable EP, an unstable limit cycle, whose maximum and minimum membrane potentials are shown on the dashed curves, and a stable limit cycle. We shall call this part of the bifurcation diagram the indented part. Finally, for $I_3 < I$ there is only a stable EP.

Figure 5*b* shows the timecourse of the membrane potential for $I_0 + I = 0$, following a hyperpolarizing step of $I(t) = -10\,\mu A\,cm^{-2}$. The effect of this current step is to switch the system from its stable EP to a stable limit cycle. The correspondence between the membrane potential of the EP and the maximum and minimum potentials of the limit cycle for $I_0 + I = 0$ is indicated by the dashed lines connecting figure 5*a,b*. Figure 5*c* shows the timecourse of the membrane potential for the stable limit cycle when the external current, $I_0 + I$, is $-2.6\,\mu A\,cm^{-2}$. Figure 5*d* shows the damped oscillation which results, following a hyperpolarizing step of $I(t) = -10\,\mu A\,cm^{-2}$, when the external current, $I_0 + I$ is $0.6\,\mu A\,cm^{-2}$.

This set of responses together with those of figure 4 are consistent with the experimental recordings of LHb neurons (Wilcox *et al.* 1988) with the possible exception of the case $I_1 < I < I_2$ where there is no stable EP and the system is in a permanent state of low threshold oscillation. This possible defect will be discussed in the next section. In addition the six dimensional model (equations (6)) fires tonically to a depolarizing current step applied when the cell is at rest (not shown). This is also found experimentally.

6. VARIATION OF PARAMETER VALUES

In Figure 6 we show the effect that varying the parameters $g_{KCa(T)}$ and k_{Ca} has on the bifurcation

PHILOSOPHICAL TRANSACTIONS OF THE ROYAL SOCIETY B BIOLOGICAL SCIENCES

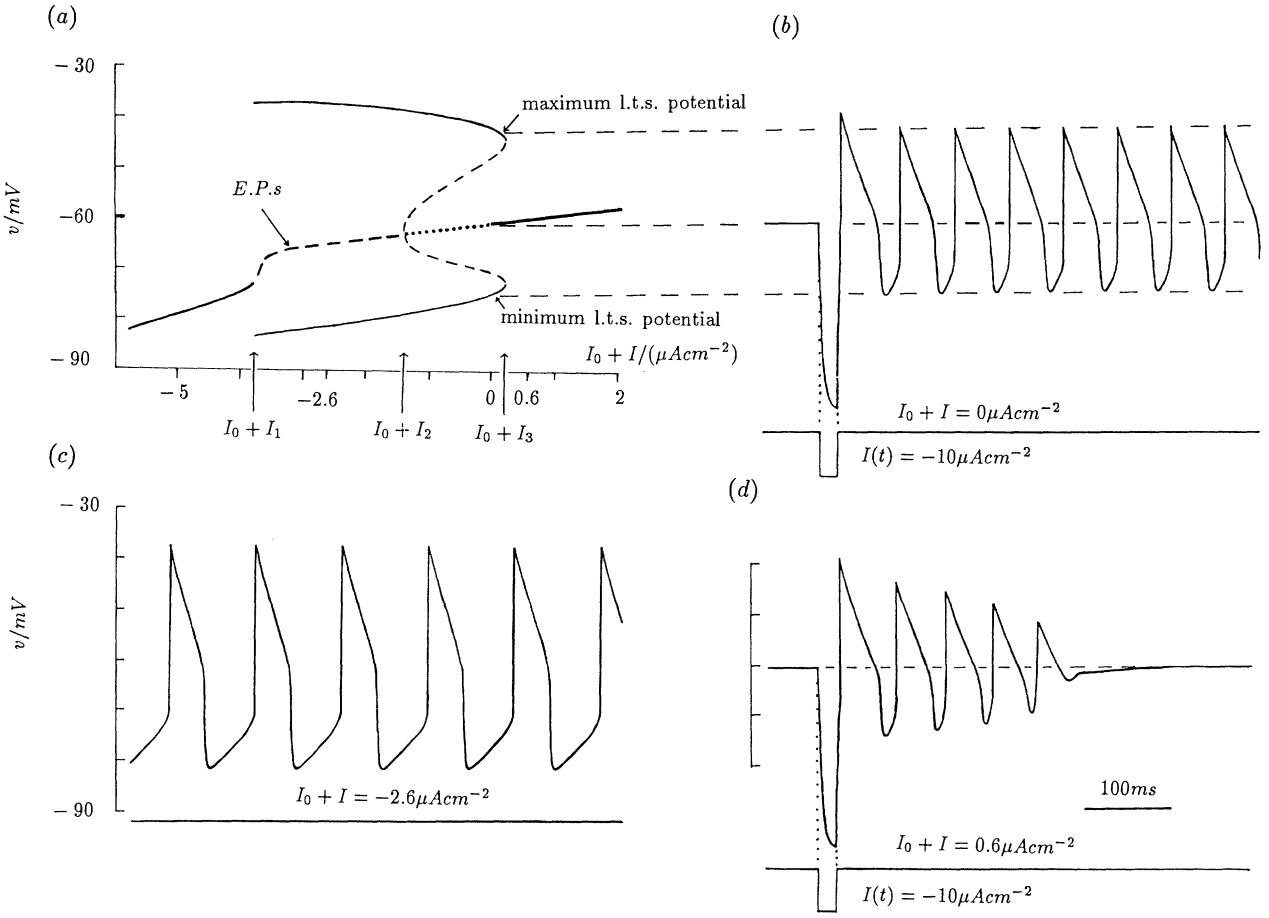

Figure 5. (*a*) $(I_0 + I, v)$ bifurcation diagram of the three-dimensional physiological model (equations (4)). As in figure 2*a* sloping line gives coordinates of EPs whose stability is indicated as follows: solid line, stable; dotted line, stable with eigenvalues of form $-\alpha \pm \imath\beta$, $-\gamma$; dashed-line, unstable. Bifurcation points occur at $I_0 + I = I_0 + I_1$, $I_0 + I_2$ and $I_0 + I_3\,\mu A\,cm^{-2}$. Unstable limit cycle solutions are indicated by the dashed curves leaving the line of EPs at $I_0 + I_2$ and terminating at $I_0 + I_3$. Stable limit cycle solutions exist between $I_0 + I_1$ and $I_0 + I_3$ as indicated by the outer solid curves. (*b*) Rebound oscillations of three-dimensional physiological model (equations (4)) to a hyperpolarizing current step of $-10\,\mu A\,cm^{-2}$ amplitude and 20 ms in duration with $I_0 + I = 0\,\mu A\,cm^{-2}$. Horizontal dashed lines connect maximum and minimum values of membrane potential with corresonding pair of points on the bifurcation diagram. (*c*) Stable limit cycle solution of equations (4) with $I_0 + I = -2.6\,\mu A\,cm^{-2}$. (*d*) Damped oscillatory solution of equations (4) following a hyperpolarizing current step of amplitude $-10\,\mu A\,cm^{-2}$ and 20 ms in duration with $I_0 + I = 0.6\,\mu A\,cm^{-2}$. Other parameter values given in Appendix 1.

diagram for equations (4). The columns have k_{Ca} varying from $0.060\,ms^{-1}$ in the left-hand column to $0.020\,ms^{-1}$ in the right-hand column and the rows have $g_{KCa(T)}$ varying from $0.6\,mS\,cm^{-2}$ at the top to $1.8\,mS\,cm^{-2}$ at the bottom. The middle diagram, figure 6*e*, is the same as figure 5*a* with $k_{Ca} = 0.044\,ms^{-1}$ and $g_{KCa(T)} = 1.2\,mS\,cm^{-2}$. Features to note are: (i) the indentation increases as k_{Ca} decreases; (ii) the indentation is similar in figure 6*b*,*d*,*f* and also for figure 6*e*,*g*; (iii) in figure 6*a* the bifurcation is supercritical with the result that for a small range of external current there are two stable limit cycles present. In all other cases the bifurcation is subcritical.

In § 3 the reason for choosing a decreased value of k_{Ca} was to increase the range of values of the external current for which the unstable limit cycle was present, that is, to increase the indentation.

A more significant change in the bifurcation diagram comes from varying the separation between the half activation points θ_{m_T} and θ_{h_T}. In the right-hand column of figure 7 these half activation points are as in equations (4). In the third column their separation has been increased by 3.4 mV by displacing them by equal amounts ($v_{sep} = 1.7$ mV) in opposite directions. In the first and second columns their separation has been increased to 6 mV ($v_{sep} =$ 3 mV: first column) and 4 mV ($v_{sep} = 2$ mV: second column) in a similar fashion. We will refer to these models, and their bifurcation diagrams, as Type A (left-hand column), Type B (second column), Type C (third column), and Type D (right-hand column).

For Type A the bifurcation diagram consists entirely of stable EPs. Nonetheless the system responds to a hyperpolarizing step with a gradually decaying low threshold oscillation (figure 7*e*). This happens when the external current, $I + I_0$, is $-1\,\mu A\,cm^{-2}$ which is in the range of external currents which, in the cases of the second and third columns, allow stable limit cycles.

For Type B all the EPs are stable and there are no Hopf bifurcations. There are stable limit cycles present for a range of external current values. In this

PHILOSOPHICAL TRANSACTIONS OF THE ROYAL SOCIETY B BIOLOGICAL SCIENCES

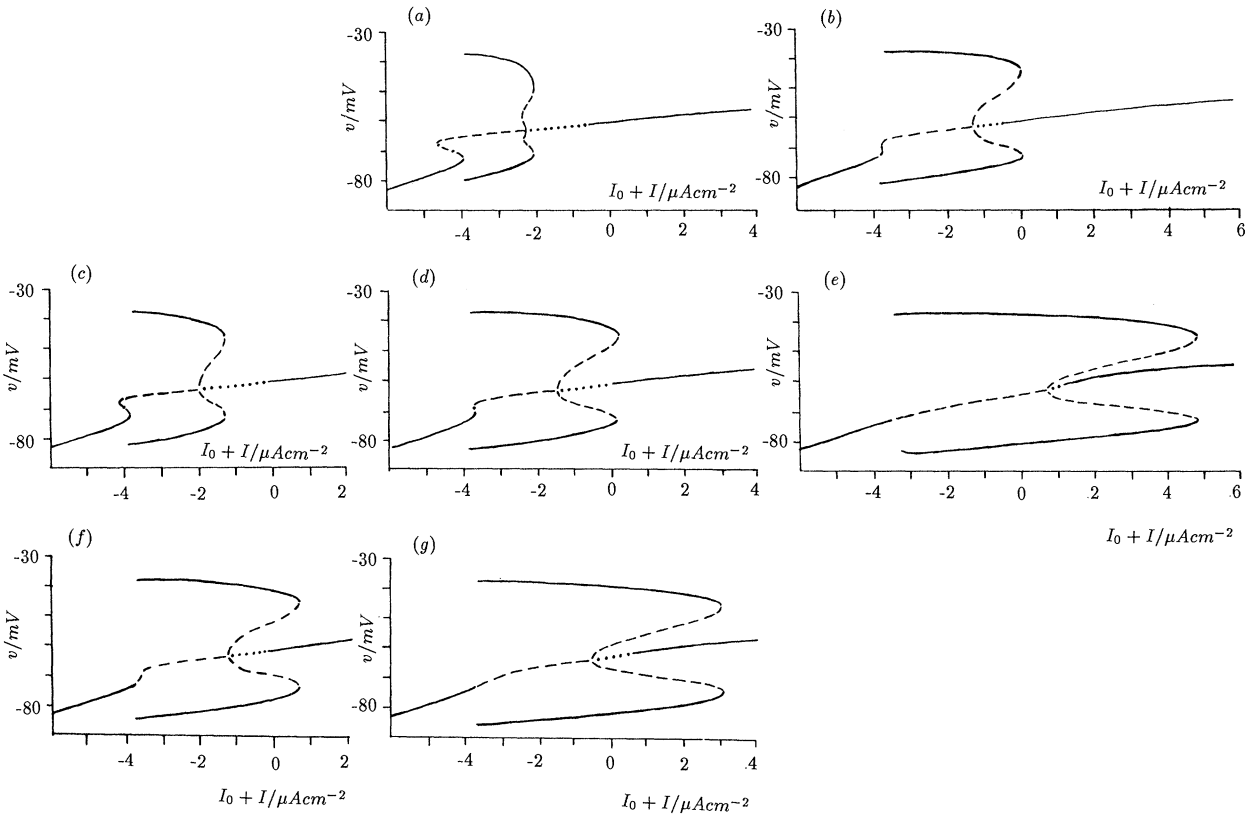

Figure 6. Bifurcation diagrams for equations (4) for different values of k_{Ca} and $g_{KCa(T)}$. Stability of limit cycle solutions and EP is as indicated in figure 5. Values for (k_{Ca} (in ms^{-1}), $g_{KCa(T)}$ (in $mS\,cm^{-2}$)) are as follows: (*a*) (0.044, 0.6), (*b*) (0.02, 0.6), (*c*) (0.06, 1.2), (*d*) (0.044, 1.2), (*e*) (0.02, 1.2), (*f*) (0.06, 1.8), (*g*) (0.044, 1.8). Other parameter values given in Appendix 1.

range a hyperpolarizing current step can drive the system into permanent oscillation (figure 7*i*). Outside this range we can obtain decaying oscillations (figure 7*f*) similar to those of figure 7*e*.

For Type C the bifurcation diagram has both stable and unstable EPs and can show decaying oscillations (figure 7*g*) or oscillations around an unstable EP (figure 7*l*). Because the bifurcation diagram is indented on both sides, the system can also give sustained oscillations following a hyperpolarizing pulse at two different levels of external current (figure 7*j*,*n*).

For Type D the bifurcation diagram includes unstable EPs and the responses are as described in figure 5. This means that the system can show either decaying oscillations (figure 7*h*), sustained oscillations following a hyperpolarizing pulse (figure 7*k*) or oscillations around an unstable EP (figure 7*m*).

This classification of bifurcation diagrams is useful in relating the physiological model to experimental observations. In the presence of tetrodotoxin (TTX) and harmaline IO cells show rebound oscillations of Type A (Yarom 1991, figure A1). In § 10 we will show that rat nRT cells (Bal & McCormick 1993) may be of Types A or B. In LHb neurons the more typical rebound response is of Type A, but Type B also occurs (Wilcox *et al.* 1988, figures 13 and 14). In the third of this series of papers (Hindmarsh & Rose 1994*b*) we will show that by decreasing k and k_{Ca} it is possible to cause a cyclical movement around the left hand end of a Type C bifurcation diagram. This gives rise to a type of spindling which is similar to that recorded from ferret nRT neurons (von Krosigk *et al.* 1993). In Hindmarsh & Rose (1994*b*) we will also show that spindling in cat TC cells could be explained by a model in which cyclical movement occurs around a Type D bifurcation diagram.

7. A MODEL OF THE TYPE D PHYSIOLOGICAL MODEL

In this section we will discuss a simplified model of the physiological model of Type D. All the bifurcation diagrams shown in this paper are experimentally observable and have one bifurcation parameter, the external current. To describe the distinctions between Types A, B, C, and D a second bifurcation parameter, v_{sep}, would be required. Although it might be desirable to have a simplified model of all four types, with two bifurcation parameters, we take a simpler approach and just choose one type. The reasons for choosing Type D are that it has a more familiar bifurcation diagram with a more varied structure, it has small unstable limit cycles, which suggest and simplify the discussion of resonance (Hindmarsh & Rose 1994*a*), and it suggests a model for intrinsic spindle generation (Hindmarsh & Rose 1994*b*).

The reason for wanting a simplified model is to provide a clearer picture of how the original model

PHILOSOPHICAL TRANSACTIONS OF THE ROYAL SOCIETY B BIOLOGICAL SCIENCES

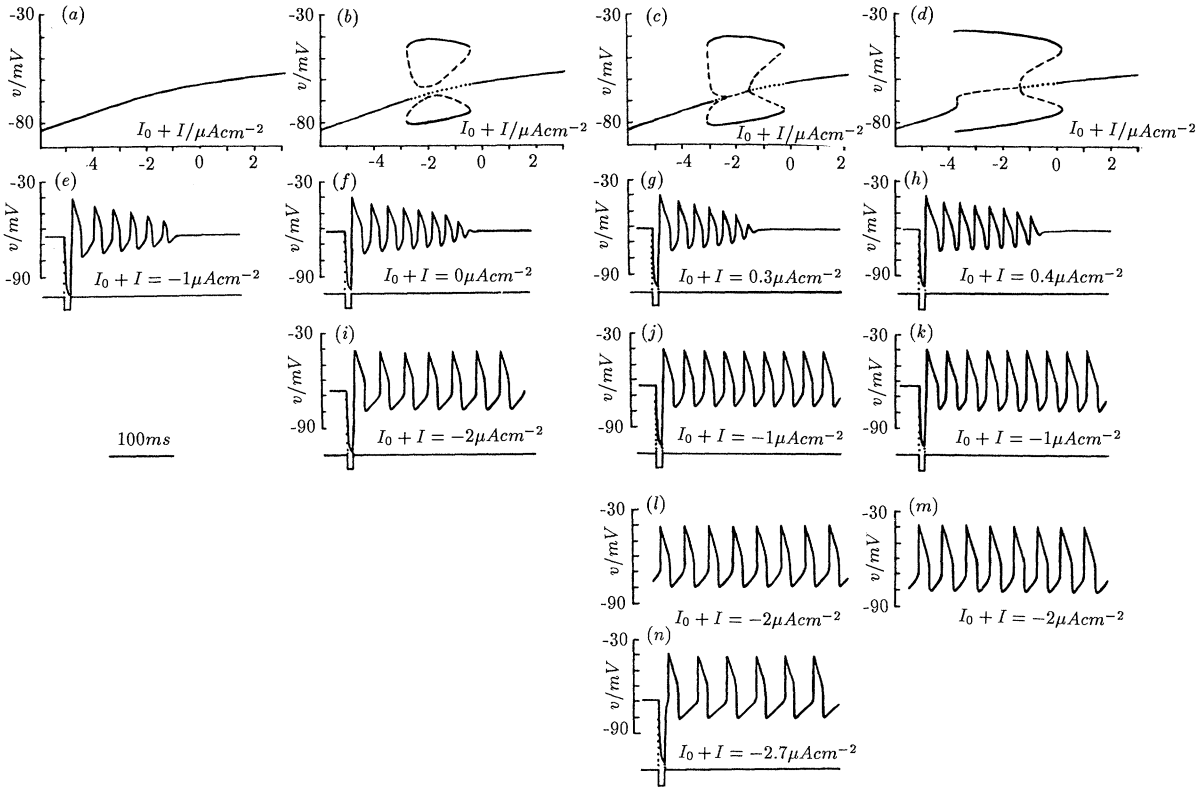

Figure 7. Bifurcation diagrams and responses to hyperpolarizing current steps (of $-10\,\mu A\,cm^{-2}$ amplitude and 20 ms in duration) for equations (4) as the separation between the half activation points θ_{m_T} and θ_{h_T} is varied. Stability of limit cycle solutions and EPs is as indicated in figure 5. (*a*) Type A bifurcation diagram with $v_{sep} = 3$ mV. All EPs are stable and the system responds, to a hyperpolarizing current step, with a decaying oscillation as shown in (*e*) where $I_0 + I = -1\,\mu A\,cm^{-2}$. (*b*) Type B bifurcation diagram with $v_{sep} = 2$ mV. All EPs are stable and the system may respond, to a hyperpolarizing current step, with either, a decaying oscillation as shown in (*f*) where $I_0 + I = 0\,\mu A\,cm^{-2}$, or a sustained oscillation as shown in (i) where $I_0 + I = -2\,\mu A\,cm^{-2}$. (*c*) Type C bifurcation diagram with $v_{sep} = 1.7$ mV. Both stable and unstable EPs are present. The system may respond to a hyperpolarizing current step, with either, a decaying oscillation as shown in (*g*) where $I_0 + I = 0.3\,\mu A\,cm^{-2}$, a sustained oscillation as shown in (*j*) where $I_0 + I = -1\,\mu A\,cm^{-2}$ or a sustained oscillation as shown in (*n*) where $I_0 + I = -2.7\,\mu A\,cm^{-2}$. For a range of external currents the cell also has permanent oscillations around an unstable EP as shown in (*l*) with $I_0 + I = -2\,\mu A\,cm^{-2}$. (*d*) Type D bifurcation diagram with $v_{sep} = 0$ mV. Both stable and unstable EPs are present. As in figure 5 the system may respond, to a hyperpolarizing current step, with either, a decaying oscillation as shown in (*h*) where $I_0 + I = 0.4\,\mu A\,cm^{-2}$, or a sustained oscillation as shown in (*k*) where $I_0 + I = -1\,\mu A\,cm^{-2}$. For a range of external currents the cell also has permanent oscillations around an unstable EP as shown in (*m*) with $I_0 + I = -2\,\mu A\,cm^{-2}$. Other parameter values given in Appendix 1.

works, for example how it responds to current steps. In equations (4) the time constants of the $\dot{h}_T$ and $\dot{c}$ equations are similar. This makes the analysis of the model more difficult that it would be if, for instance, one of them was much slower than the other. Our approach is to construct a qualitatively similar system. This will concentrate on the structure of the dynamical system that we think is responsible for these low threshold oscillations. To simplify the discussion we define the vector $\boldsymbol{v}$ by:

$$\boldsymbol{v} = \begin{pmatrix} v \\ h_T \\ c \end{pmatrix},$$

so that equations (4) may be written as:

$$\dot{\boldsymbol{v}} = \boldsymbol{F}(\boldsymbol{v}) + \boldsymbol{f}(t),$$

where $\boldsymbol{f}(t)$ represents the variable external current so that

$$\boldsymbol{f}(t) = C^{-1}\begin{pmatrix} I + I(t) \\ 0 \\ 0 \end{pmatrix},$$

and where $\boldsymbol{F}(\boldsymbol{v})$ represents the remaining terms on the right hand side of equations (4) including the constant external term I_0.

To improve the agreement between the model of the model and the physiological model we have chosen $I_0 = -1.35\,\mu A\,cm^{-2}$ so that the EP (when $I + I(t) = 0$) is close to the bifurcation point labelled $I_0 + I_2$ in figure 5*a*. Let this EP be at $\boldsymbol{v}_0$ so that $\boldsymbol{F}(\boldsymbol{v}_0) = \boldsymbol{O}$. Put:

$$\boldsymbol{w} = \boldsymbol{v} - \boldsymbol{v}_0, \qquad (8)$$

PHILOSOPHICAL TRANSACTIONS OF THE ROYAL SOCIETY B BIOLOGICAL SCIENCES

and equations (7) become:

$$\begin{aligned}\dot{\boldsymbol{w}} = \dot{\boldsymbol{v}} &= \boldsymbol{F}(\boldsymbol{v}) + \boldsymbol{f}(t),\\ &= \boldsymbol{F}(\boldsymbol{v}_0 + \boldsymbol{w}) + \boldsymbol{f}(t),\\ &= \boldsymbol{A}\boldsymbol{w} + \boldsymbol{H}(\boldsymbol{w}) + \boldsymbol{f}(t),\end{aligned}$$

where $\boldsymbol{A} = \boldsymbol{DF}(\boldsymbol{v}_0)$ is the linear approximation matrix and $\boldsymbol{H}(\boldsymbol{w})$ are the higher order terms. The matrix $\boldsymbol{A}$ has one real eigenvalue $-\gamma$ and a complex conjugate pair $-\alpha \pm \imath\beta$, where α, β and γ are positive. Now transform to a real canonical form of $\boldsymbol{A}$ using the transformation $\boldsymbol{T}$:

$$\boldsymbol{T}\dot{\boldsymbol{w}} = \boldsymbol{T}\boldsymbol{A}\boldsymbol{T}^{-1}\boldsymbol{T}\boldsymbol{w} + \boldsymbol{T}\boldsymbol{H}(\boldsymbol{T}^{-1}\boldsymbol{T}w) + \boldsymbol{T}f(t),$$

or

$$\dot{\boldsymbol{x}} = \boldsymbol{A}_c\boldsymbol{x} + \boldsymbol{H}_c(\boldsymbol{x}) + \boldsymbol{T}\boldsymbol{f}(t),$$

where

$$\boldsymbol{x} = \boldsymbol{T}\boldsymbol{w}, \tag{9}$$

and $\boldsymbol{A}_c$ is a real canonical form of $\boldsymbol{A}$ and $\boldsymbol{H}_c(\boldsymbol{x}) = \boldsymbol{T}\boldsymbol{H}(\boldsymbol{T}^{-1}\boldsymbol{x})$. This can be written as:

$$\left.\begin{aligned}\dot{x} &= -\alpha x + \beta y + H_{c1}(x,y,z) + T_{11}(I + I(t)),\\ \dot{y} &= -\beta x - \alpha y + H_{c2}(x,y,z) + T_{21}(I + I(t)),\\ \dot{z} &= -\gamma z + H_{c3}(x,y,z) + T_{31}(I + I(t)).\end{aligned}\right\} \tag{10}$$

Our simplified model of equations (10) is obtained by replacing the higher order terms $\boldsymbol{H}_c$ so that these equations become:

$$\left.\begin{aligned}\dot{x} &= -\alpha x + \beta y - \alpha(a(x^2 + y^2) - bz)x\\ &\quad + T_{11}(I + I(t)),\\ \dot{y} &= -\beta x - \alpha y - \alpha(a(x^2 + y^2) - bz)y\\ &\quad + T_{21}(I + I(t)),\\ \dot{z} &= -\gamma z + \gamma(c(x^2 + y^2) - d(x^2 + y^2)^2)\\ &\quad + T_{31}(I + I(t)),\end{aligned}\right\} \tag{11}$$

where the values of the positive constants a, b, c, d are given in Appendix 2. The reasons for choosing these values are given in §9. To see how these equations approximate the previous equations we consider the case where $I + I(t) = 0$. Using polar coordinates (r, θ) instead of (x, y), equations (11) become:

$$\left.\begin{aligned}\dot{r} &= -\alpha r(1 + ar^2 - bz),\\ \dot{\theta} &= -\beta,\\ \dot{z} &= -\gamma(z - cr^2 + dr^4).\end{aligned}\right\} \tag{12}$$

Consider the first of equations (12) in which z may be regarded as a parameter. For $z < 1/b$ this equation has a stable EP at $r = 0$, whereas for $z > 1/b$ it has a stable EP at $r = \sqrt{[(bz - 1)/a]}$ and an unstable EP at $r = 0$. Combine this equation for $\dot{r}$ with the equation for $\dot{\theta}$, and these stable equilibrium solutions become a stable EP at the origin and a stable limit cycle respectively. They will correspond to the resting EP shown in figure 4*a* and the stable limit cycle shown in figure 4*a*. Clearly z is a variable playing a role similar to that of c in equations (4).

The solutions of the three-dimensional system of equations (12) may now be described. First note that the simple form of the equation for $\dot{\theta}$ means that these solutions have constant angular velocity around the cylindrical axis $r = 0$. This means that the behaviour of the solutions is determined by the two-dimensional subsystem consisting of the equations for $\dot{r}$ and $\dot{z}$.

The nullclines for these equations are shown in figure 8*d* which also shows their intersections at the EPs L, M and H. The lower EP, L, at the origin is stable and corresponds to the stable EP of the three-dimensional system. The middle and higher EPs, M and H, are unstable and stable respectively and correspond to an unstable limit cycle and stable limit cycle of the three-dimensional system.

Next consider the case where $I \neq 0$ and $I(t) = 0$. The effect of non-zero I in equations (11) is to displace their EP from $\boldsymbol{O}$, when $I = 0$, to $\boldsymbol{x}(I)$. A first approximation to $\boldsymbol{x}(I)$ is:

$$\begin{pmatrix} x(I)\\ y(I)\\ z(I)\end{pmatrix} = I\begin{pmatrix} (\alpha T_{11} + \beta T_{21})/(\alpha^2 + \beta^2)\\ (-\beta T_{11} + \alpha T_{21})/(\alpha^2 + \beta^2)\\ T_{31}/\gamma\end{pmatrix}. \tag{13}$$

Once again we change coordinates in order to move the EP back to $\boldsymbol{O}$. This time by the substitution:

$$\boldsymbol{x} = \boldsymbol{x}(I) + \bar{\boldsymbol{x}}, \tag{14}$$

in equations (11). We now note that α may be made as small as we wish by choosing I_0 so that the EP is close to the bifurcation point, I may be restricted to small values and γ is smaller than β. In addition to these small terms we see from equations (13) that $x(I)$ and $y(I)$ are also small but $z(I)$ is not.

Therefore having made the substitution (14) we disregard all terms with products of two or more of these small terms. In this way equations (11) become:

$$\left.\begin{aligned}\dot{\bar{x}} &= -\alpha\bar{x} + \beta\bar{y} - \alpha(a(\bar{x}^2 + \bar{y}^2) - b(\bar{z} + IT_{31}/\gamma))\bar{x},\\ \dot{\bar{y}} &= -\beta\bar{x} - \alpha\bar{y} - \alpha(a(\bar{x}^2 + \bar{y}^2) - b(\bar{z} + IT_{31}/\gamma))\bar{y},\\ \dot{\bar{z}} &= -\gamma\bar{z} + \gamma(c(\bar{x}^2 + \bar{y}^2) - d(\bar{x}^2 + \bar{y}^2)^2).\end{aligned}\right\} \tag{15}$$

Using polar coordinates $\bar{r}$, $\bar{\theta}$, instead of $\bar{x}$, $\bar{y}$, equations (15) become:

$$\left.\begin{aligned}\dot{\bar{r}} &= -\alpha\bar{r}(1 + a\bar{r}^2 - b(\bar{z} + IT_{31}/\gamma)),\\ \dot{\bar{\theta}} &= -\beta,\\ \dot{\bar{z}} &= -\gamma(\bar{z} - c\bar{r}^2 + d\bar{r}^4).\end{aligned}\right\} \tag{16}$$

Equations (16) are the same as equations (12), except for the appearance of the term IT_{31}/γ, and the behaviour of their solutions may be discussed, as above, by reference to the two-dimensional subsystem consisting of the equations for $\dot{\bar{r}}$ and $\dot{\bar{z}}$. This subsystem is:

$$\begin{aligned}\dot{\bar{r}} &= -\alpha\bar{r}(1 + a\bar{r}^2 - b(\bar{z} + IT_{31}/\gamma)),\\ \dot{\bar{z}} &= -\gamma(\bar{z} - c\bar{r}^2 + d\bar{r}^4),\end{aligned} \tag{17}$$

PHILOSOPHICAL TRANSACTIONS OF THE ROYAL SOCIETY B BIOLOGICAL SCIENCES

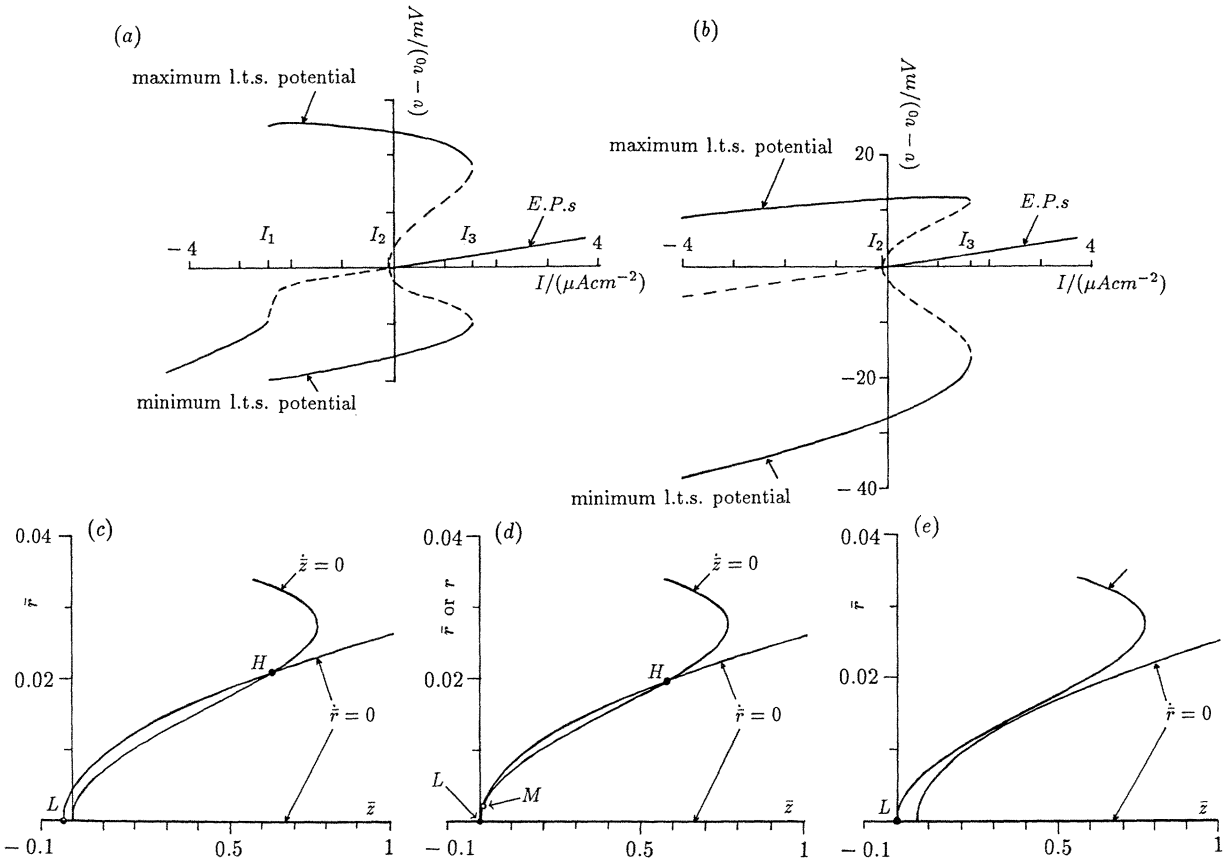

Figure 8. (*a*) $(I, v-v_0)$ bifurcation diagram calculated numerically for the three-dimensional physiological model (equations (4)). This diagram is the same as figure 5*a* with the axes repositioned so that the origin corresponds to the point $(I_0+I, v) = (-1.35\,\mu A\,cm^{-2}, -63.26\,mV)$ in figure 5*a*. There are three bifurcation points at $I=I_1$, I_2 and I_3. (*b*) $(I, v-v_0)$ bifurcation diagram of the model of the model calculated analytically as described in §9. The bifurcation points at I_2 and I_3 occur at similar values to I_2 and I_3 in (*a*). In (*a*) and (*b*) stability of EPs and limit cycles indicated by: dashed line, unstable; solid line, stable. (*c*)–(*e*) Nullcline diagrams for the model of the model calculated using equations (18) for (*c*) $I=-1\,\mu A\,cm^{-2}$, (*d*) $I=0\,\mu A\,cm^{-2}$ and (*e*) $I=2\,\mu A\,cm^{-2}$. Parameter values for the model of the model are given in Appendix 2.

and the $\bar{r}$ and $\bar{z}$ nullclines for these equations are:

$$\bar{z} = (1+a\bar{r}^2)/b - IT_{31}/\gamma,$$
$$\bar{z} = c\bar{r}^2 - d\bar{r}^4, \qquad (18)$$

respectively.

Clearly the position of the $\bar{r}$ nullcline will change with I and the direction of this change will depend on the sign of T_{31}. For the transformation $\boldsymbol{T}$ we have used (see Appendix 2) this sign is negative.

Thus the effect of increasing I is to translate the $\bar{r}$ nullcline to the right. Figure 6*c*–*e* shows the nullclines in the $(\bar{z}, \bar{r})$ plane for the cases (*c*) $I<I_2$, (*d*) $I=0$ and (*e*) $I>I_3$. The equilibrium points, lower, middle and higher, are labelled L, M and H. In figure 8*d* L and H are stable and M is unstable. In figure 8*c* L is unstable and H is stable. In figure 8*e* L is stable.

8. SWITCHING BETWEEN THE EP AND THE LIMIT CYCLE

We will now discuss how the switching between a stable EP and a stable limit cycle by means of positive and negative applied currents steps, as shown in figure 4*b* is explained by the model of the model. Note that this comparison is only qualitative. We describe the changes in the configuration of the nullclines of the model of the model as the bifurcation points at $I=I_1$, I_2 and I_3 are crossed when $I(t)$ is changed. We do not match the values of I or of $I(t)$ when making the comparison.

Suppose the system, with $I=0$ and $I(t)=0$ is in equilibrium at point L of figure 8*d*. If a negative current step, $I(t)<0$ is applied, then the nullcline diagram changes from figure 8*d* to figure 8*c* and the state of the system changes to the EP at H in figure 8*c*. This corresponds to a stable limit cycle for the three-dimensional system. If the current step is now terminated, so $I(t)=0$, the system changes its state to the stable EP at H in figure 8*d*. Thus the effect of a sufficiently long and prolonged negative current step is to switch the three-dimensional system from its stable EP to its stable limit cycle.

The physiological model would behave similarly to this if $I(t)$ were sufficiently prolonged so that the external current was such that $I_1 < I+I(t) < I_2$. In this case oscillations would build up after a delay following the application of a current step. In the example given in figure 4*b*, the negative change in $I(t)$ is larger in amplitude so that $I+I(t)<I_1$, and

the membrane potential is stable during the application of the current step. This does not happen with the model of the model because it does not have a stable EP for negative values of I, as will be seen in the next section (compare figures 6*a* and 6*b*).

Now suppose the system, with $I = 0$ and $I(t) = 0$, is in the EP at H of figure 8*d*. If a positive current step is applied then the nullcline diagram changes from figure 8*d* to figure 8*e* and the state of the system changes to the stable EP at L in figure 8*e*. If the current step is now terminated the system changes its state to the stable EP at L in figure 8*d*. Thus the effect of a sufficiently long and prolonged positive current step is to switch the three-dimensional system from its stable limit cycle to its stable EP.

This explains, qualitatively at least, why a positive current step applied to the physiological model, as shown in figure 4*b*, had the effect of terminating the limit cycle.

We have considered the case which allows a limit cycle when there is no external current. From the observations of Wilcox *et al.* (1988), this case is found less commonly than cells which show a damped oscillation of three to four cycles. An interesting feature predicted by the model of the model occurs when the parameters are such that the limit cycle only just fails to appear. In saying that the limit cycle only just fails to appear we mean that the $\bar{r}$ and $\bar{z}$ nullclines, that are shown intersecting at M and H in figure 8*d*, no longer intersect but still lie close together (similar to figure 8*e*). A consequence of this is that following a negative current step the system is not held in a limit cycle but returns to the stable EP. In so doing the phase point representing the state of the system returns through the narrow channel between the nullclines. Being close to both nullclines its movement is slow, which means that the oscillation of the three-dimensional system is slow to decay.

9. THE BIFURCATION DIAGRAM

We now choose the values of a, b, c, d so that the bifurcation diagram predicted by the model of the model is in at least approximate agreement with that of the physiological model.

To obtain the bifurcation diagram, from the model of the model, we need, for each value of I, the $(\bar{z}, \bar{r})$ coordinates of the EPs of equations (17). These are given by the points of intersection of the nullclines whose equations are (18). Therefore the $\bar{r}$ coordinates of these EPs satisfy:

$$bd\bar{r}^4 + (a - bc)\bar{r}^2 + (1 - Ib\,T_{31}/\gamma) = 0. \tag{19}$$

The number of positive real roots will depend on I. For values of I, for which there are two positive roots, these roots are given by

$$\bar{r}_\pm = \sqrt{\left(\frac{bc - a \pm \sqrt{((a - bc)^2 - 4bd(1 - Ib\,T_{31}/\gamma))}}{2bd}\right)} \tag{20}$$

and the corresponding values of $\bar{z}$ by:

$$\bar{z}_\pm = c\bar{r}_\pm^2 - d\bar{r}_\pm^4. \tag{21}$$

For the stable limit cycle through $(\bar{r}_+, \bar{z}_+)$ the corresponding membrane potential, is obtained from transformations (8), (9), (14), which give:

$$\boldsymbol{v} = \boldsymbol{v}_0 + \boldsymbol{w} = \boldsymbol{v}_0 + \boldsymbol{T}^{-1}\boldsymbol{x} = \boldsymbol{v}_0 + \boldsymbol{T}^{-1}(\boldsymbol{x}(I) + \bar{\boldsymbol{x}}),$$

and so the membrane potential is:

$$v = v_0 + T_{11}^{-1}(x(I) + \bar{x}) + T_{12}^{-1}(y(I) + \bar{y}) + T_{13}^{-1}(z(I) + \bar{z}). \tag{22}$$

Because $T_{12}^{-1} = 0$ and, for the limit cycle through $(\bar{r}_+, \bar{z}_+)$, $\bar{x}(= \bar{r}\cos\bar{\theta})$ varies between $\bar{r}_+$ and $-\bar{r}_+$, we find that the maximum and minimum values for the membrane potential are given by:

$$\left.\begin{aligned} v_{\max} &= v_0 + T_{11}^{-1}(x(I) + \bar{r}_+) + T_{13}^{-1}(z(I) + \bar{z}_+), \\ v_{\min} &= v_0 + T_{11}^{-1}(x(I) - \bar{r}_+) + T_{13}^{-1}(z(I) + \bar{z}_+). \end{aligned}\right\} \tag{23}$$

By subtraction equations (23) give:

$$v_{\max} - v_{\min} = 2\,T_{11}^{-1}\bar{r}_+.$$

Similarly for the unstable limit cycle through $(\bar{r}_-, \bar{z}_-)$ we have:

$$v_{\max} - v_{\min} = 2\,T_{11}^{-1}\bar{r}_-.$$

From the bifurcation diagram of the physiological model, shown in figure 8*a*, we see that the left hand bifurcation point occurs when $I = I_2 = -0.074\,\mu\mathrm{A\,cm^{-2}}$. At this point $\bar{r}_- = 0$ and so $1 - I_A b\,T_{31}/\gamma = 0$ giving $b = \gamma/(I_A\,T_{31}) \approx 450$.

For the stable limit cycle, at the same current value, we have:

$$(v_{\max} - v_{\min})_2 = 2\,T_{11}^{-1}\bar{r}_+ = 2\,T_{11}^{-1}\sqrt{[(bc - a)/(bd)]}. \tag{24}$$

At the other end of the bifurcation diagram, where the stable and unstable limit cycles meet, $I = I_3 = 1.5\,\mu\mathrm{A\,cm^{-2}}$. At this point $\bar{r}_+ = \bar{r}_-$ so:

$$(a - bc)^2 = 4bd(1 - I_3 b\,T_{31}/\gamma), \tag{25}$$

and:

$$(v_{\max} - v_{\min})_3 = 2\,T_{11}^{-1}\bar{r}_+ = 2\,T_{11}^{-1}\sqrt{[(bc - a)/(2bd)]}. \tag{26}$$

From figure 8*a* we obtain:

$$\left.\begin{aligned} (v_{\max} - v_{\min})_2 &= 40.5\,\mathrm{mV}, \\ (v_{\max} - v_{\min})_3 &= 27.7\,\mathrm{mV}. \end{aligned}\right\} \tag{27}$$

From (24), (25), (27) and using the value found above for b, we obtain:

$$d = \frac{64(T_{11}^{-1})^4(1 - I_3 b\,T_{31}/\gamma)}{b(v_{\max} - v_{\min})_2^4} \approx 1.3 \times 10^6.$$

Also from (24) and (26) we obtain:

$$(v_{\max} - v_{\min})_2 = (v_{\max} - v_{\min})_3\sqrt{2},$$

a prediction which is correct to within 2 mV. Finally from (25), and the values found above for b and d, we have:

$$a - bc \approx 230\,000. \tag{28}$$

In theory it should be possible to obtain the value of c from the equation:

$$v_{\max} + v_{\min} - 2T_{13}^{-1}(z(I) + \bar{z}_+),$$

obtained from adding equations (23), and using (13) and (21). But the quantity $v_{\max} + v_{\min}$ is near zero and sensitive to the values of $v_{\max}$ and $v_{\min}$. Thus small departures in the values of $v_{\max}$ and $v_{\min}$ from the idealized behaviour assumed for the model of the model can produce a large change in the value of c and also of a which is then obtained using (28).

We need an alternative way to find the value of c. The following method is inspired by the voltage clamp technique.

Suppose that, for the system of equations (12), the value of r were fixed at r', then the value of z would change according to:

$$\dot{z} = -\gamma(z - cr'^2 + dr'^4), \tag{29}$$

which means that $z(t) \to cr'^2 + dr'^4$ as $t \to \infty$. By observing this limiting value of $z(t)$ for various values of r' we can estimate the value of c.

The way we do this is to take the initial state:

$$\boldsymbol{x}' = \begin{pmatrix} r' \\ 0 \\ 0 \end{pmatrix},$$

and then use the transformations (8) and (9) to find the corresponding initial state:

$$\boldsymbol{v}' = \boldsymbol{v}_0 + \boldsymbol{w} = \boldsymbol{v}_0 + \boldsymbol{T}^{-1}\boldsymbol{x}',$$

of equations (4). We then integrate equations (4) forward through one time step to obtain the later state $\boldsymbol{v}''$. This is transformed back via transformations (8) and (9) to the corresponding state:

$$\boldsymbol{x}'' = \boldsymbol{T}(\boldsymbol{v}'' - \boldsymbol{v}_0) = \begin{pmatrix} x'' \\ y'' \\ z'' \end{pmatrix}.$$

If we define $r'' = \sqrt{[(x''^2 + y''^2)]}$ then in general we will find that $r'' \neq r'$ and the new state does not lie on the cylinder $r = r'$. We now apply the (clamping) constraint, that it does lie on this cylinder, by changing (x'', y'', z'') to $(x''r'/r'', y''r'/r'', z')$. Continuing this process we can find the limiting value of z for $r = r'$. Using (29) and then (28) we obtain $c = 2000$ and $a = 670\,000$.

Using these values for a, b, c and d the bifurcation diagram for the model of the model is as shown in figure 8*b*. This should be compared with the bifurcation diagram for the physiological model shown in figure 8*a*. Although the asymmetry of the bifurcation diagram of the model of the model is in the wrong direction and there is no bifurcation point at I_1 this diagram has two important features. It is a good approximation near the bifurcation point at I_2 and its other bifurcation point is close to I_3. The first of these features will be important in the following paper (Hindmarsh & Rose 1994*a*) and the second in the final paper (Hindmarsh & Rose 1994*b*).

10. COMPARISON WITH OTHER MODELS

In the above physiological model of § 3 we used a comparatively simple description of I_T. We now show that similar conclusions are reached if we add $I_{KCa(T)}$ to more detailed models such as those of Wang (1994) and Wang *et al.* (1991) Modification of these models enables us to predict the result of voltage clamp experiments more accurately.

First we will describe a four-dimensional model based on our original thalamic model (Rose & Hindmarsh 1989*a–c*) and the work of Wang (1994). We start with equations (1) and discard the A-current (see § 1) but this time retain the fast sodium current $I_{Na} = g_{Na}m^3h(v - v_{Na})$. In our thalamic model (Rose & Hindmarsh 1989*a–c*) we approximated the sodium inactivation variable h by $0.85 - 3n^4$ (in the case where $I_A = 0$), and the activation variable m by m_∞. We also added a persistent sodium current $I_{NaP} = g_{NaP}m_{NaP_\infty}(v - v_{Na})$ (which we wrote as $I_{S_b} = g_{S_b}s_{b_\infty}(v - v_{Na})$). Including I_{Na}, with this approximation for h, gives us a system of equations:

$$\left.\begin{aligned} \dot{v} &= C^{-1}\{-I_{Na} - I_K - I_L - I_T - I_{NaP} + I_{Ext}\}, \\ \dot{n} &= \tau_n^{-1}(v)(n_\infty(v) - n), \\ \dot{h}_T &= \tau_{h_T}^{-1}(h_{T_\infty}(v) - h_T), \end{aligned}\right\} \tag{30}$$

where $I_{Na} = g_{Na}m_\infty^3(v)(0.85 - 3n^4)(v - v_{Na})$, $I_K = g_K n^4(v - v_K)$, $I_T = g_T m_{T_\infty}(v)h_T(v - v_{Ca})$, $I_L = g_L(v - v_L)$, and $I_{NaP} = g_{NaP}m_{NaP_\infty}(v - v_{Na})$. Although we could use these equations we prefer to work from equations of Wang (1994) which more accurately reflect the experimental data. Wang's equations are:

$$\left.\begin{aligned} \dot{v} &= C^{-1}\{-I_{Na} - I_K - I_L - I_T - I_{NaP} \\ &\quad - I_H + I_{Ext} + I(t)\}, \\ \dot{n} &= \phi_n\tau_n^{-1}(v)(n_\infty(v) - n), \\ \dot{h}_T &= \phi_{h_T}\tau_{h_T}^{-1}(v)(h_{T_\infty}(v) - h_T), \\ \dot{m}_H &= \phi_{m_H}\tau_{m_H}^{-1}(v)(m_{H_\infty}(v) - m_H), \end{aligned}\right\} \tag{31}$$

where $I_{Na} = g_{Na}m_\infty^3(v)(0.85 - n)(v - v_{Na})$, $I_K = g_K n^4(v - v_K)$, $I_T = g_T m_{T_\infty}^3(v)h_T(v - v_{Ca})$, $I_L = g_L(v - v_L)$, $I_H = g_H m_H^2(v - v_H)$, $I_{NaP} = g_{NaP}m_{NaP_\infty}^3(v - v_{Na})$ and ϕ_n, ϕ_{h_T} and ϕ_{m_H} are temperature factors which scale the time constants of n, h_T and m_H respectively.

The main differences, apart from a more informed choice of parameter values, are that the sodium inactivation variable h is approximated by $0.85 - n$, the T-current activation variable $m_{T_\infty}(v)$ appears as $m_{T_\infty}^3(v)$, the time constant for the T-current inactivation variable is voltage dependent and there is an additional current I_H. These changes were based on voltage clamp experiments published after our thalamic model was first described.

Removing I_H and adding $I_{KCa(T)}$ gives us the

PHILOSOPHICAL TRANSACTIONS OF THE ROYAL SOCIETY B BIOLOGICAL SCIENCES

four-dimensional system of equations:

$$\left.\begin{aligned} \dot{v} &= C^{-1}\{-I_{\mathrm{Na}} - I_{\mathrm{K}} - I_{\mathrm{L}} - I_{\mathrm{T}} - I_{\mathrm{NaP}} \\ &\quad - I_{\mathrm{KCa(T)}} + I_{\mathrm{Ext}} + I(t)\}, \\ \dot{n} &= \phi_n \tau_n^{-1}(v)(n_\infty(v) - n), \\ \dot{h}_{\mathrm{T}} &= \phi_{h_{\mathrm{T}}} \tau_{h_{\mathrm{T}}}^{-1}(v)(h_{\mathrm{T}_\infty}(v) - h_{\mathrm{T}}), \\ \dot{c} &= -kI_{\mathrm{T}} - k_{\mathrm{Ca}} c. \end{aligned}\right\} \quad (32)$$

To confirm the similarity between the solutions of these equations and those of the three-dimensional model of § 3 we repeat the experiment described in figure 4. Starting with the system at rest a hyperpolarizing current pulse drives the system into continuous bursting which may be terminated by applying a depolarizing current pulse. The very similar result in the present case is shown in figure 9*a*. In figure 9*b* we show an example of a prediction of a voltage clamp experiment using this model in which the voltage is stepped from a holding potential of −90 mV to −40 mV. The cell has been treated with TTX ($g_{\mathrm{Na}} = g_{\mathrm{NaP}} = 0\,\mu\mathrm{A\,cm^{-2}}$) and the clamp current is leak subtracted. For purposes of comparison with real cells we have added a differential equation for m_{T} (see Appendix 3). The total current consists of three components, I_{K} (shown dotted), I_{T} and $I_{\mathrm{KCa(T)}}$. Note that the total current has both inward and outward components. Subtracting I_{K} from the total current we obtain $I_{\mathrm{T}} + I_{\mathrm{KCa(T)}}$ shown as the solid curve in figure 9*c*. If all K^+ currents are blocked we obtain the same timecourse of I_{T} (figure 9*c*, lower dotted curve). Subtraction of I_{T} from the current shown by the solid curve in figure 9*c* gives $I_{\mathrm{KCa(T)}}$ (figure 9*c*, upper dotted curve). In figure 9*d*, I_{T} and $I_{\mathrm{KCa(T)}}$ are redrawn and the maximum value of $I_{\mathrm{KCa(T)}}$ is labelled I_1. The value of I_{T} when $I_{\mathrm{KCa(T)}}$ has this maximum value is labelled I_2. By measurement of I_1 and I_2 together with the time constant of decay of $I_{\mathrm{KCa(t)}}$ we can deduce the value of k_{Ca} as explained in § 11 below.

In figure 10, which may be compared to figure 7, the columns correspond to different values of the separation between the half activation points, $\theta_{m_{\mathrm{T}}}$ and $\theta_{h_{\mathrm{T}}}$, of m_{T} and h_{T}. The top row shows the bifurcation diagrams of Types A, B and C for the system in the case $g_{\mathrm{Na}} = 0$ and $g_{\mathrm{NaP}} = 0$. To look for the existence of one of these bifurcation diagrams experimentally the following procedure should be adopted. Block the sodium currents with TTX. Then for each value of the external current (horizontal axis) determine whether or not the cell has a resting potential (stable EP). Next, by applying current pulses of varying magnitudes, determine whether or not the cell has any sustained oscillations. The magnitude of

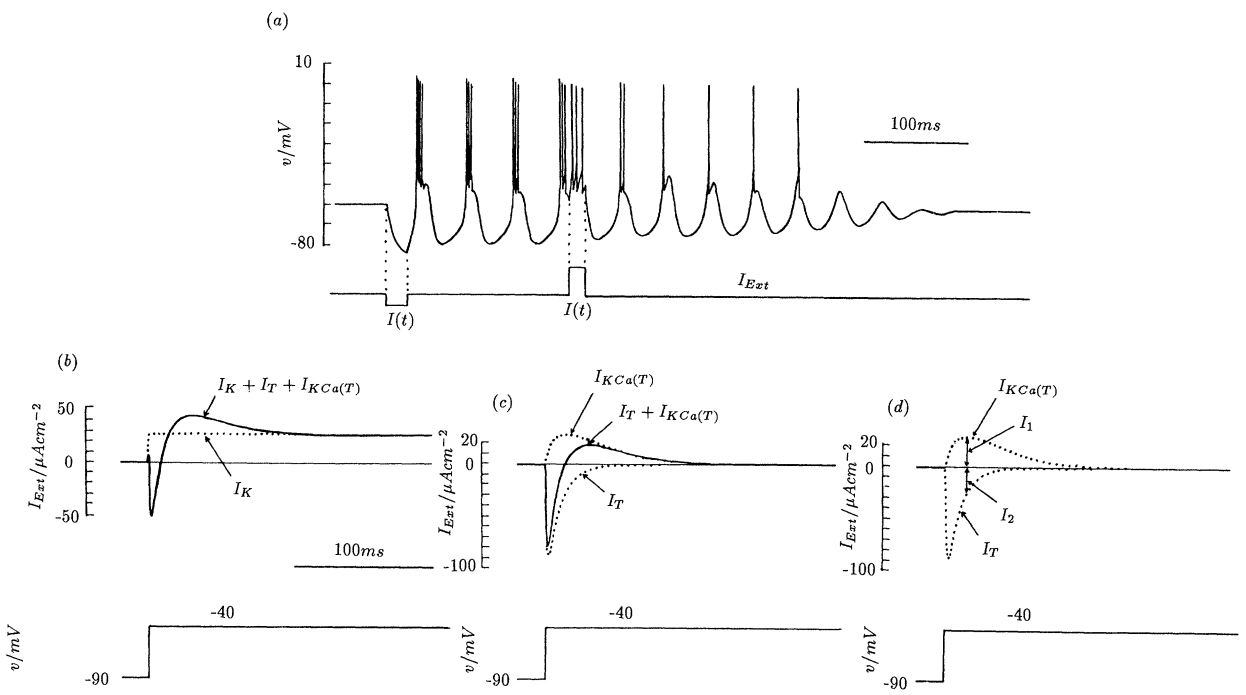

Figure 9. (*a*) Numerical solution of equations (32) with $I_{\mathrm{Ext}} = 1.5\,\mu\mathrm{A\,cm^{-2}}$. A hyperpolarizing current step, $I(t)$, of amplitude $-3\,\mu\mathrm{A\,cm^{-2}}$ and 20 ms in duration, is followed by a depolarizing current step, $I(t)$, of amplitude $8\,\mu\mathrm{A\,cm^{-2}}$ and 15 ms in duration. The time interval between the onset of the hyperpolarizing current step and the onset of the depolarizing current step was 175 ms. (*b*)–(*d*) Analysis of voltage clamp experiment for the model described by equations (32) with a differential equation for m_{T} added (see Appendix 3). (*b*) For a voltage clamp step from −90 mV to −40 mV in the presence of TTX ($g_{\mathrm{Na}} = g_{\mathrm{NaP}} = 0\,\mathrm{mS\,cm^{-2}}$), the clamp current (solid curve) consists of $I_{\mathrm{K}} + I_{\mathrm{T}} + I_{\mathrm{KCa(T)}}$ when the leakage current, I_{L}, is subtracted. Dotted curve shows timecourse of I_{K}. (*c*) Subtraction of I_{K} from the current trace shown in (*b*) gives the clamp current for $I_{\mathrm{T}} + I_{\mathrm{KCa(T)}}$ (solid curve). Also shown separately are I_{T} and $I_{\mathrm{KCa(T)}}$ (dotted curves). (*d*) Measurement of I_1 and I_2 from the clamp currents for I_{T} and $I_{\mathrm{KCa(T)}}$ (dotted curves). See § 11 for calculations involving I_1 and I_2. Parameter values given in Appendix 3.

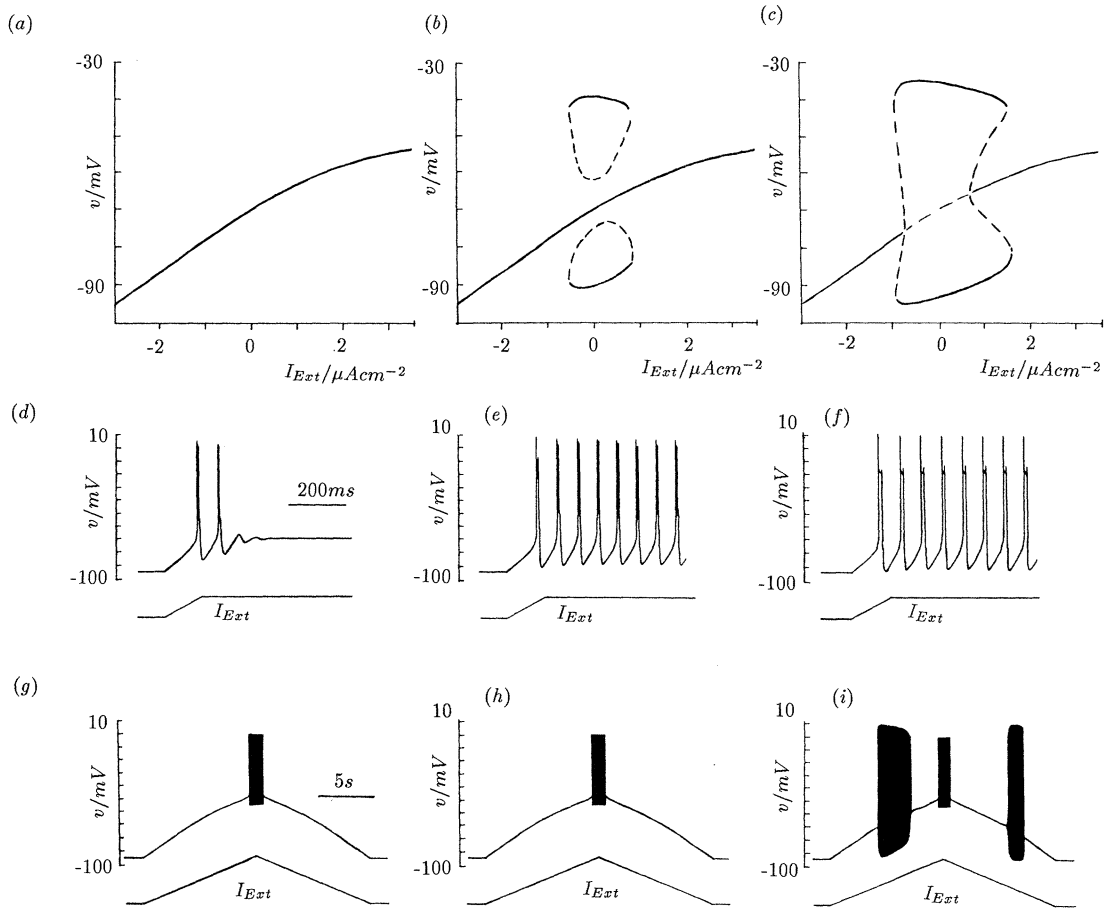

Figure 10. Bifurcation diagrams and responses to current ramps for equations (32) as the separation between the half activation points θ_{m_T} and θ_{h_T} is varied. Bifurcation diagrams are plotted for a cell treated with TTX ($g_{Na} = g_{NaP} = 0\,mS\,cm^{-2}$). Stability of limit cycle solutions and EPs is as indicated in figure 5 except that EPs are simply indicated as stable (solid curve) or unstable (dashed curve). (*a*) Type A bifurcation diagram with $v_{sep} = 2\,mV$. (*b*) Type B bifurcation diagram with $v_{sep} = 1\,mV$. (*c*) Type C bifurcation diagram with $v_{sep} = 0\,mV$. (*d*) to (*f*) Responses to a fast current ramp of equations (32) (no TTX) for cells whose bifurcation diagrams (with TTX) are as shown in (*a–c*). The current rises from $I_{Ext} = -3\,\mu A\,cm^{-2}$ to $I_{Ext} = 0\,\mu A\,cm^{-2}$ in 150 ms and is then maintained. (*g–i*) Responses to a slow current ramp of equations (32) (no TTX) for cells whose bifurcation diagrams (with TTX) are as shown in (*a–c*). The current rises from $I_{Ext} = -3\,\mu A\,cm^{-2}$ to $I_{Ext} = 4\,\mu A\,cm^{-2}$ in 10 s and then falls to $I_{Ext} = -3\,\mu A\,cm^{-2}$ in the next 10 s. Parameter values given in Appendix 3.

the resting potential (if any) and the maximum and minimum potentials of these oscillation (if any) are then plotted (vertical axis). Note however that only the solid curves are determined by this procedure.

Two further experimental predictions are shown in figure 10. These serve to distinguish between the cases described in the three columns. In the third row figure 10*g–i* shows the effect of applying a slow rising and falling current ramp to each of the three cases. As would be expected, from the bifurcation diagrams of figures 10*a* and *b*, a slowly changing current results in a slowly changing resting potential with the exception of the tonic firing at the peak of the ramp. The presence of unstable EPs in the (asymmetric) bifurcation diagram figure 10*c* results in asymmetric bursting on the rise and fall as shown in figure 10*i*. Thus the slow ramp serves to distinguish the first two columns from the third.

The second row, figure 10*d–f*, shows the effect of applying a current which rises rapidly until the first low threshold spike is fired at which point it is held constant. This distinguishes the first column from the second and third because the low threshold oscillation in the first column is not sustained. This is as expected from the bifurcation diagram of figure 10*a* which shows no stable limit cycles.

Guided by the results of figure 10 we are able to relate the model given by equations (32) to the firing patterns of nRT cells as described by Bal & McCormick (1993). We chose a separation, between the half activation points θ_{m_T} of m_T and θ_{h_T} of h_T, that was intermediate between the separations chosen for the first and second columns of figure 10. We also lowered the half activation point of m_{NaP} by 7 mV and increased g_K from $15\,mS\,cm^{-2}$ to $25\,mS\,cm^{-2}$.

With these changes this four-dimensional model responds in a similar way to the observations shown in figure 3 of Bal & McCormick (1993). As the background current is increased the decay takes longer and the burst frequency increases until a point is reached where the rebound bursting gives way to a tonic tail of single spike activity terminated by a damped oscillatory return to a stable EP (figure 11*c–f*).

In the presence of TTX ($g_{Na} = g_{NaP} = 0$) sustained oscillations occur for a small range of external currents

and, as shown in figure 11*a*, the corresponding bifurcation diagram is of Type B, despite the fact that the full system does not show sustained oscillations. Note that a reduction of the separation (v_{sep}) of about 1 mV is sufficient produce a Type C bifurcation diagram (figure 11*b*) suggesting that cells of Type C could be present in the reticularis nucleus. This possibility will be explored further in the final paper (Hindmarsh & Rose 1994*b*).

Finally we report the effect of adding I_K and $I_{KCa(T)}$ to the model of Wang *et al.* (1991). In this model the inactivation gate for I_T is described by a two step kinetic scheme in order to account for slow recovery from inactivation. Our purpose is to show that the mechanism we have proposed for rebound low threshold oscillations will still operate with this slow recovery from inactivation. The equations for this modification of the model of Wang *et al.* (1991) are:

$$\left.\begin{aligned} \dot{v} &= C^{-1}\{-I_T - I_K - I_L - I_{KCa(T)} + I_{Ext}\},\\ \dot{m}_T &= \tau_{m_T}^{-1}(v)(m_{T_\infty}(v) - m_T),\\ \dot{h} &= \alpha_1(1-h-d) - \beta_1 h,\\ \dot{d} &= \beta_2(1-h-d) - \alpha_2 h,\\ \dot{c} &= -kI_T - k_{Ca}c, \end{aligned}\right\} \quad (33)$$

where $I_T = g_T m_T^3 h(v - v_{Ca})$. Further details are given in Appendix 4.

In figure 12 we see that the bifurcation diagram (figure 12*a*) is similar to that of our original model as is the rebound bursting from a hyperpolarizing step (figure 12*b*). In figure 12*c–e* we repeat the voltage clamp experiment, shown previously in figure 9*b–d*. Comparing this (figure 12*d*) with our previous model (figure 9*c*) we note that the slow decay of I_T reduces the outward phase of the combined current. Thus $I_{KCa(T)}$ appears, in the outward phase, as a small current even though it has made a significant change to the bifurcation diagram.

11. ANALYSIS OF THE VOLTAGE CLAMP

In this section we show how the parameters k and k_{Ca} of equations (32) and (33) can be measured from the voltage clamp experiments shown in figures 9*b* and 12*c*. At this stage the analysis does not take into account other voltage- or calcium-dependent currents (e.g. Pennefather *et al.* 1985) which might be present in the real cell.

The timecourses of I_T and $I_{KCa(T)}$ shown in figure 9*d* may be obtained analytically as follows. The timecourse of the current I_T depends on the

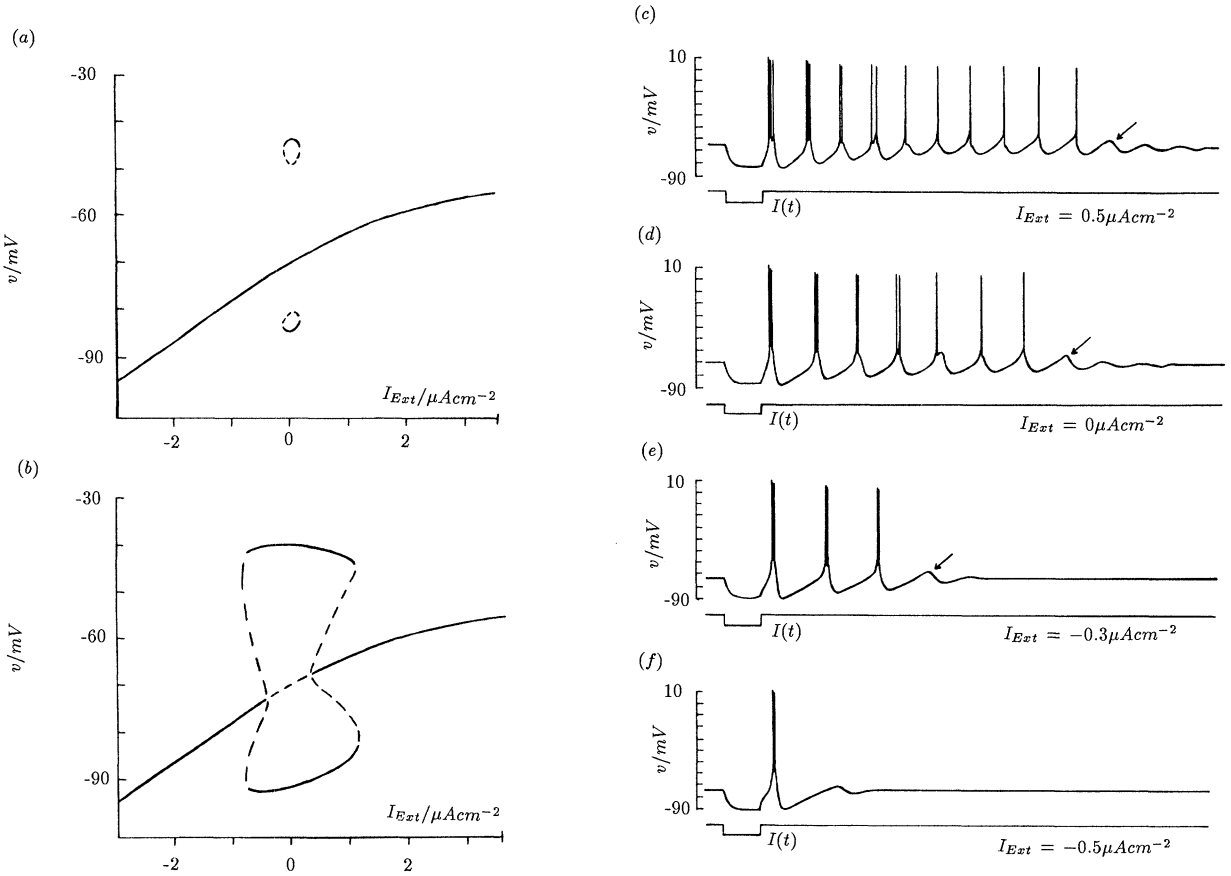

Figure 11. Model of nRT cell with parameter values given in Appendix 3. (*a*) Bifurcation diagram for the cell shown in (*c*)–(*f*) treated with TTX ($g_{Na} = g_{NaP} = 0\,mS\,cm^{-2}$). Here $v_{sep} = 1.45\,mV$ and the stability of limit cycle solutions and EPs is as indicated in figure 10. (*b*) Bifurcation diagram for the cell having the same parameter values as the cell shown in (*a*) except that $v_{sep} = 0.45\,mV$. (*c*)–(*f*) Numerical solution of equations (32) (no TTX) for $I_{Ext} = 0.5\,\mu A\,cm^{-2}$ in (*c*), $0\,\mu A\,cm^{-2}$ in (*d*), $-0.3\,\mu A\,cm^{-2}$ in (*e*) and $-0.5\,\mu A\,cm^{-2}$ in (*f*), and a hyperpolarizing current step of amplitude $-2\,\mu A\,cm^{-2}$ and 60 ms in duration. Arrows indicate damped oscillation at the end of the rebound sequence.

PHILOSOPHICAL TRANSACTIONS OF THE ROYAL SOCIETY B BIOLOGICAL SCIENCES

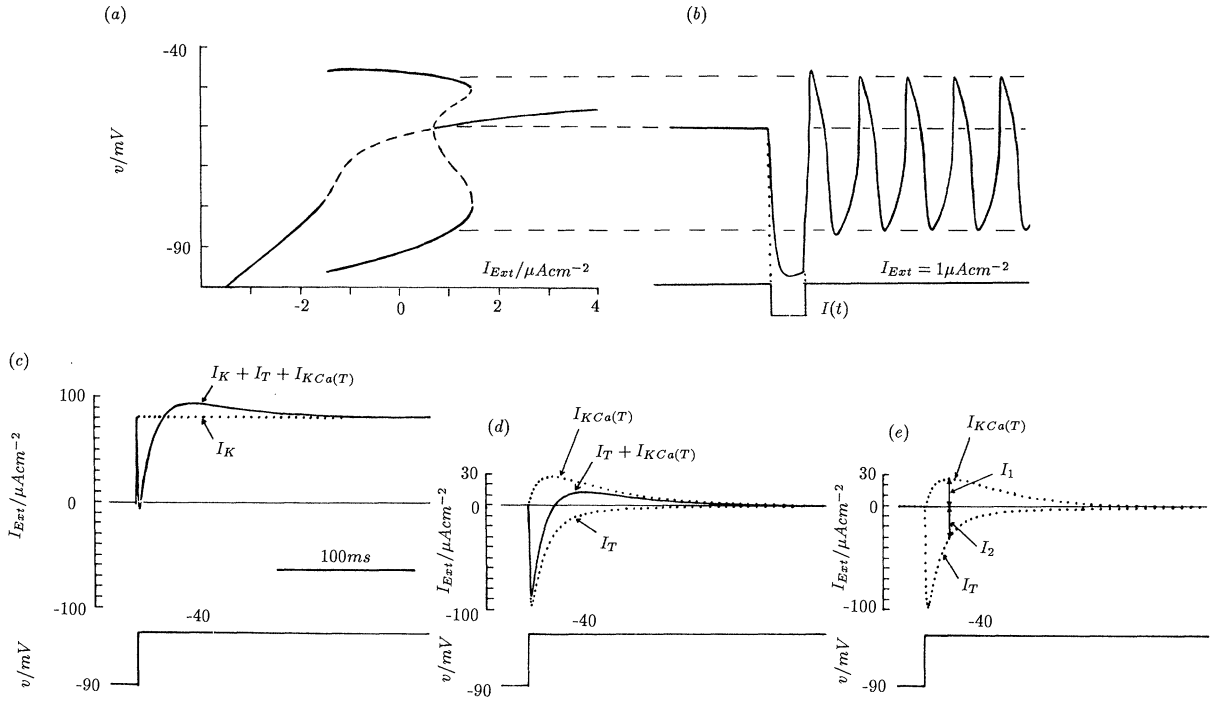

Figure 12. (*a*) Bifurcation diagram for equations (33) with parameter values given in Appendix 4 and stability of limit cycle solutions and EPs as indicated in figure 10. (*b*) An example of rebound bursting following a hyperpolarizing current step of amplitude $-4\,\mu A\,cm^{-2}$ and 50 ms in duration with $I_{Ext} = 1\,\mu A\,cm^{-2}$. (*c*)–(*d*) Analysis of voltage clamp experiment for the model described by equations (33). (*c*) For a voltage clamp step from -90 mV to -40 mV the clamp current (solid curve) consists of $I_K + I_T + I_{KCa(T)}$ when the leakage current, I_L, is subtracted. Dotted curve shows timecourse of I_K. (*d*) Subtraction of I_K from the current trace shown in (*c*) gives the clamp current for $I_T + I_{KCa(T)}$ (solid curve). Also shown separately are I_T and $I_{KCa(T)}$ (dotted curves). (*e*) Measurement of I_1 and I_2 from the clamp currents for I_T and $I_{KCa(T)}$ (dotted curves). See § 11 for calculations involving I_1 and I_2.

timecourses of $m_T(t)$ and $h_T(t)$ and is given by:

$$I_T = g_T m_T(t)^3 h_T(t)(v - v_{Ca}).$$

On clamping, from -90 mV to -40 mV, $m_T(t)$ changes exponentially from its value before the clamp, which is $m_{T_\infty}(-90) = 0$, to $m_{T_\infty}(-40) = 1$, and $h_T(t)$ changes exponentially from $h_{T_\infty}(-90) = 1$ to $h_{T_\infty}(-40) = 0$, with time constants $\tau_{m_T}(-40)$ and $\tau_{h_T}(-40)$ respectively. Thus the timecourse of I_T is given by:

$$I_T(t) = g_T(1 - \exp(-\tau_{m_T}^{-1}(-40)t)^3 \times \exp(-\tau_{h_T}^{-1}(-40)t)(-40 - v_{Ca}).$$

Knowing the timecourse of I_T we can obtain the timecourse of the concentration of intracellular free calcium c from the differential equation:

$$\dot{c} = -kI_T - k_{Ca}c.$$

Before the clamp $I_T = 0$ (as $m_{T_\infty}(-90) = 0$) and so $c = 0$. Therefore $c(t)$ is given by:

$$c(t) = \exp(-k_{Ca}t) \int_0^t \exp(k_{Ca}s)(-kI_T(s))\,ds.$$

Finally the time course of $I_{KCa(T)}$ is given by:

$$I_{KCa(T)}(t) = g_{KCa(T)} \frac{c(t)}{K_{Ca(T)} + c(t)}(-40 - v_K).$$

Because $k_{Ca} < \tau_{h_T}^{-1}(-40) < \tau_{m_T}^{-1}(-40)$ the timecourse of $c(t)$ eventually decays exponentially with time constant k_{Ca}^{-1}. As it decays $c(t)$ becomes small so that $K_{Ca(T)} + c(t) \approx K_{Ca(T)}$ and so $I_{KCa(T)}(t)$ also decays with time constant k_{Ca}^{-1}. So from the timecourse of $I_{KCa(T)}(t)$ we can measure k_{Ca}^{-1}.

To obtain k we note that the timecourses of $I_{KCa(T)}(t)$ and $c(t)$ have maximum values at the same time t_{max}. Let $I_1 = I_{KCa(T)}(t_{max})$, $I_2 = I_T(t_{max})$ and $c_{max} = c(t_{max})$. Then from the definition of $I_{KCa(T)}$ and the differential equation for c we have:

$$I_1 = g_{KCa(T)} \frac{c_{max}}{K_{Ca(T)} + c_{max}}(-40 - v_K),$$

$$0 = \dot{c}(t_{max}) = -kI_2 - k_{Ca}c_{max}.$$

From this we obtain:

$$k = \frac{-k_{Ca}K_{Ca(T)}I_1}{I_2(g_{KCa(T)}(-40 - v_K) - I_1)},$$

which allows k_{Ca} to be estimated provided that we know $g_{KCa(T)}$ and $K_{Ca(T)}$.

In the argument given above the precise details of the timecourses of $m_T(t)$ and $h_T(t)$ do not matter and so the method of estimating k and k_{Ca} applies to both of the models discussed in § 10. For these two models the currents I_1 and I_2 are indicated in figures 9*d* and 12*e*.

12. CONCLUSION

Over the past decade there has been a rapid expansion in the number of descriptions of the electrophysiological properties of different mammalian neurons (reviewed by Llinás 1988). In this paper we have attempted to organize and simplify some of these descriptions by introducing a classification scheme based on the type of bifurcation diagram produced by a one parameter (v_{sep}) family of models. The bifurcation diagram is experimentally measurable and can be related to the properties of the cells. These include cells in the lateral habenula nucleus (Wilcox *et al.* 1989) and nucleus reticularis thalami (Avanzini *et al.* 1988; Bal & McCormick 1993). Our classification could probably be extended to other neurons such as those of the inferior olivary nucleus (Yarom 1991) and paraventricular nucleus (Tasker & Dudek 1991). Further applications will be given in the last of this series of papers (Hindmarsh & Rose 1994*b*). Our aim has not been to produce a biophysically exact model for any particular cell, but to find the underlying dynamical system and present it in such a way that it can be readily modified following further experimental results. This led to the representation of the solutions of the three-dimensional physiological model on a surface resembling a paraboloid and the introduction of the model of the model. We have also predicted the outcome of voltage clamp experiments to determine the parameter values of the $\dot{c}$ equation. Together with the measurement of I_K, I_T and I_L this should make it possible to verify the model experimentally.

We introduced the simplified model of the model not just as purely qualitative model but as an approximation to the physiological model. In this paper we have used this model of the model to explain how the system responds to applied current pulses. In the following paper (Hindmarsh & Rose 1994*a*) we will use it to describe resonance analytically, and in the final paper (Hindmarsh & Rose 1994*b*) we will use it to describe intrinsic spindling in thalamocortical cells.

This work was supported by the Wellcome Trust.

APPENDIX 1. EQUATIONS AND PARAMETER VALUES FOR THE PHYSIOLOGICAL MODEL

The equations are:

$$\dot{v} = C^{-1}\{-I_{Na} - I_K - I_L - I_T - I_{KCa(T)} + I_0 + I + I(t)\},$$

$$\dot{m} = \tau_m^{-1}(v)(m_\infty(v) - m),$$

$$\dot{h} = \tau_h^{-1}(v)(h_\infty(v) - h),$$

$$\dot{n} = \tau_n^{-1}(v)(n_\infty(v) - n),$$

$$\dot{h}_T = \tau_{h_T}^{-1}(h_{T_\infty}(v) - h_T),$$

$$\dot{c} = -kg_T m_{T_\infty}(v) h_T (v - v_{Ca}) - k_{Ca} c,$$

where

$C = 1\,\mu F\,cm^{-2}$, $I_{Na} = g_{Na} m^3 h(v - v_{Na})$, $I_K = g_K n^4 (v - v_K)$, $I_T = g_T m_{T_\infty}(v) h_T (v - v_{Ca})$, $I_L = g_L(v - v_L)$, and $I_{KCa(T)} = g_{KCa(T)}(c/K_{Ca(T)} + c)(v - v_K)$.

For I_{Na}:

$$\alpha_m(v) = \frac{-(v + 29.7)/10}{\exp\{-(v + 29.7)/10\} - 1},$$

$$\beta_m(v) = 4\exp\{-(v + 54.7)/10\},$$

$$m_\infty(v) = \frac{\alpha_m(v)}{\alpha_m(v) + \beta_m(v)},$$

$$\tau_m(v) = \frac{T_m}{\alpha_m(v) + \beta_m(v)},$$

$$\alpha_h(v) = 0.07\exp\{-(v + 48)/20\},$$

$$\beta_h(v) = \frac{1}{\exp\{-(v + 18)/10\} + 1},$$

$$h_\infty(v) = \frac{\alpha_h(v)}{\alpha_h(v) + \beta_h(v)},$$

$$\tau_h(v) = \frac{T_h}{\alpha_h(v) + \beta_h(v)},$$

and $T_m = 0.26$, $T_h = 0.26$, $g_{Na} = 120\,mS\,cm^{-2}$, $v_{Na} = 55\,mV$.

For I_K:

$$\alpha_n(v) = \frac{-(v + 45.7)/100}{\exp\{-(v + 45.7)/10\} - 1},$$

$$\beta_n(v) = 0.125\exp\{-(v + 55.7)/80\},$$

$$n_\infty(v) = \frac{\alpha_n(v)}{\alpha_n(v) + \beta_n(v)},$$

$$\tau_n(v) = \frac{T_n}{\alpha_n(v) + \beta_n(v)},$$

and $T_n = 0.009$, $g_K = 10\,mS\,cm^{-2}$, $v_K = -90\,mV$.

For I_T:

$$m_{T_\infty}(v) = \frac{1}{1 + \exp\{-\gamma_{m_T}(v - \theta_{m_T} - v_{sep})\}}$$

$$h_{T_\infty}(v) = \frac{1}{1 + \exp\{-\gamma_{h_T}(v - \theta_{h_T} + v_{sep})\}}$$

and $\gamma_{m_T} = 0.6\,mV^{-1}$, $\theta_{m_T} = -64.5\,mV$, $\gamma_{h_T} = -0.5\,mV^{-1}$, $\theta_{h_T} = -70\,mV$, $\tau_{h_T}^{-1} = 0.045\,ms^{-1}$, $g_T = 0.6\,mS\,cm^{-2}$, $v_{Ca} = 130\,mV$. For the Type D model $v_{sep} = 0\,mV$.

For $I_{KCa(T)}$:

$k = 0.001\,\mu M\,cm^{-2}\,\mu A^{-1}\,ms^{-1}$, $k_{Ca} = 0.044\,ms^{-1}$, $g_{KCa(T)} = 1.2\,mS\,cm^{-2}$, $K_{Ca(T)} = 1\,\mu M$, $v_K = -90\,mV$.

For I_L:

$g_L = 0.25\,mS\,cm^{-2}$ and $v_L = -59\,mV$.

The value of I_0 is $-1.35\,\mu A\,cm^{-2}$ and the relevant values of I and $I(t)$ are given in the text and the figure legends.

The simplifications of this model have the same parameter values when the cell is not subject to an

PHILOSOPHICAL TRANSACTIONS OF THE ROYAL SOCIETY B BIOLOGICAL SCIENCES

external current with the following changes:

Five-dimensional thalamic model (figure 1*d–f*):

$g_{\mathrm{KCa(T)}} = 0\,\mathrm{mS\,cm^{-2}}$.

Three-dimensional model (figures 4*a*,*b*, 5 and 6*a*):

$g_{\mathrm{Na}} = 0\,\mathrm{mS\,cm^{-2}}$.

Two-dimensional thalamic model (figures 1*a–c* and 2):

$g_{\mathrm{Na}} = g_{\mathrm{KCa(T)}} = 0\,\mathrm{mS\,cm^{-2}}$.

APPENDIX 2. EQUATIONS AND PARAMETER VALUES FOR THE MODEL OF THE MODEL

The equations for the model of the three-dimensional physiological model of Type D (defined in Appendix 1), are:

$$\dot{\bar{x}} = -\alpha\bar{x} + \beta\bar{y} - \alpha(a(\bar{x}^2 + \bar{y}^2) - b(\bar{z} + IT_{31}/\gamma))\bar{x},$$

$$\dot{\bar{y}} = -\beta\bar{x} - \alpha\bar{y} - \alpha(a(\bar{x}^2 + \bar{y}^2) - b(\bar{z} + IT_{31}/\gamma))\bar{y},$$

$$\dot{\bar{z}} = -\gamma\bar{z} + \gamma(c(\bar{x}^2 + \bar{y}^2) - d(\bar{x}^2 + \bar{y}^2)^2).$$

These equations model the physiological model Type D in the case where the EP is at $v_0 = -63.26\,\mathrm{mV}$ with $I = 0$. At this EP the eigenvalues are $-\alpha \pm \imath\beta$, $-\gamma$ where:

$\alpha = 0.02098, \quad \beta = 0.26295, \quad \gamma = 0.02089.$

Also the values of a, b, c and d are (see text):

$a = 670\,000, \quad b = 450, \quad c = 2000, \quad d = 1\,300\,000.$

The transformation matrices $\boldsymbol{T}$, $\boldsymbol{T}^{-1}$ are not uniquely determined. The values that we used were:

$$\boldsymbol{T} = \begin{pmatrix} 0.00099 & 0.00625 & 0.00997 \\ 0.00018 & 0.29914 & -0.10876 \\ -0.00062 & 0.48187 & 0.76919 \end{pmatrix}.$$

$$\boldsymbol{T}^{-1} = \begin{pmatrix} 1000 & 0 & -12.96369 \\ -0.24868 & 2.72274 & 0.38820 \\ 0.96379 & -1.70570 & 1.04640 \end{pmatrix}.$$

APPENDIX 3. EQUATIONS AND PARAMETER VALUES FOR THE FOUR-DIMENSIONAL MODEL

The equations are:

$$\dot{v} = C^{-1}\{-I_{\mathrm{Na}} - I_{\mathrm{K}} - I_{\mathrm{L}} - I_{\mathrm{T}} - I_{\mathrm{NaP}} - I_{\mathrm{KCa(T)}} + I_{\mathrm{Ext}} + I(t)\},$$

$$\dot{n} = \phi_n\tau_n^{-1}(v)(n_\infty(v) - n),$$

$$\dot{h}_{\mathrm{T}} = \phi_{h_{\mathrm{T}}}\tau_{h_{\mathrm{T}}}^{-1}(v)(h_{\mathrm{T}_\infty}(v) - h_{\mathrm{T}}),$$

$$\dot{c} = -kI_{\mathrm{T}} - k_{\mathrm{Ca}}c,$$

where

$C = 1\,\mu\mathrm{F\,cm^{-2}}$, $I_{\mathrm{Na}} = g_{\mathrm{Na}}m_\infty^3(v)(0.85 - n)(v - v_{\mathrm{Na}})$, $I_{\mathrm{K}} = g_{\mathrm{K}}n^4(v - v_{\mathrm{K}})$, $I_{\mathrm{T}} = g_{\mathrm{T}}m_{\mathrm{T}_\infty}^3(v)h_{\mathrm{T}}(v - v_{\mathrm{Ca}})$, $I_{\mathrm{L}} = g_{\mathrm{L}}(v - v_{\mathrm{L}})$, $I_{\mathrm{NaP}} = g_{\mathrm{NaP}}m_{\mathrm{NaP}_\infty}^3(v - v_{\mathrm{Na}})$, and $I_{\mathrm{KCa(T)}} = g_{\mathrm{KCa(T)}}(c/K_{\mathrm{Ca(T)}} + c)(v - v_{\mathrm{K}})$.

For I_{Na}:

$$\alpha_m(v) = \frac{-0.1(v + 29.7 - \sigma_{\mathrm{Na}})}{\exp\{-0.1(v + 29.7 - \sigma_{\mathrm{Na}})\} - 1},$$

$$\beta_m(v) = 4\exp\{-(v + 54.7 - \sigma_{\mathrm{Na}})/18\},$$

$$m_\infty(v) = \frac{\alpha_m(v)}{\alpha_m(v) + \beta_m(v)},$$

and $g_{\mathrm{Na}} = 10\,\mathrm{mS\,cm^{-2}}$, $v_{\mathrm{Na}} = 55\,\mathrm{mV}$, $\sigma_{\mathrm{Na}} = 10\,\mathrm{mV}$.

For I_{K}:

$$\alpha_n(v) = \frac{-0.01(v + 45.7 - \sigma_{\mathrm{K}})}{\exp\{-0.1(v + 45.7 - \sigma_{\mathrm{K}})\} - 1},$$

$$\beta_n(v) = 0.125\exp\{-(v + 55.7 - \sigma_{\mathrm{K}})/80\},$$

$$n_\infty(v) = \frac{\alpha_n(v)}{\alpha_n(v) + \beta_n(v)},$$

$$\tau_n(v) = \frac{1}{\alpha_n(v) + \beta_n(v)},$$

and $g_{\mathrm{K}} = 15\,\mathrm{mS\,cm^{-2}}$, $v_{\mathrm{K}} = -105\,\mathrm{mV}$, $\phi_n = 28.57$, $\sigma_{\mathrm{K}} = 10\,\mathrm{mV}$.

For I_{NaP}:

$$\alpha_{\mathrm{NaP}}(v) = \frac{-0.1(v + 29.7 - \sigma_{\mathrm{NaP}})}{\exp\{-0.1(v + 29.7 - \sigma_{\mathrm{NaP}})\} - 1},$$

$$\beta_{\mathrm{NaP}}(v) = 4\exp\{-(v + 54.7 - \sigma_{\mathrm{NaP}})/18\},$$

$$m_{\mathrm{NaP}_\infty}(v) = \frac{\alpha_{\mathrm{NaP}}(v)}{\alpha_{\mathrm{NaP}}(v) + \beta_{\mathrm{NaP}}(v)},$$

and $g_{\mathrm{NaP}} = 7\,\mathrm{mS\,cm^{-2}}$, $v_{\mathrm{Na}} = 55\,\mathrm{mV}$, $\sigma_{\mathrm{NaP}} = -5\,\mathrm{mV}$.

For I_{T}:

$$m_{\mathrm{T}_\infty}(v) = \frac{1}{1 + \exp\{-(v - \theta_{m_{\mathrm{T}}} - v_{\mathrm{sep}})/7.8\}},$$

$$h_{\mathrm{T}_\infty}(v) = \frac{1}{1 + \exp\{(v - \theta_{h_{\mathrm{T}}} - v_{\mathrm{sep}})/5},$$

$$\tau_{h_{\mathrm{T}}}(v) = h_{\mathrm{T}_\infty}(v)\exp\{(v + 162.5)/17.8\} + 20,$$

and $g_{\mathrm{T}} = 1\,\mathrm{mS\,cm^{-2}}$, $v_{\mathrm{Ca}} = 120\,\mathrm{mV}$, $\phi_{h_{\mathrm{T}}} = 2$, $\theta_{m_{\mathrm{T}}} = -65\,\mathrm{mV}$, $\theta_{h_{\mathrm{T}}} = -79\,\mathrm{mV}$.

For I_{L}:

$g_{\mathrm{L}} = 0.12\,\mathrm{mS\,cm^{-2}}, \quad v_{\mathrm{L}} = -70\,\mathrm{mV}.$

For $I_{\mathrm{KCa(T)}}$:

$g_{\mathrm{KCa(T)}} = 1.2\,\mathrm{mS\,cm^{-2}}$, $v_{\mathrm{K}} = -105\,\mathrm{mV}$, $k = 0.001\,\mu\mathrm{M\,cm^{-2}\,\mu A^{-1}\,ms^{-1}}$, $k_{\mathrm{Ca}} = 0.044\,\mathrm{ms^{-1}}$, $K_{\mathrm{Ca(T)}} = 1\,\mu\mathrm{M}$.

The relevant values of I_{Ext}, $I(t)$ and v_{sep} are given in the text and the figure legends.

In the voltage clamp experiment described in § 10, and shown in figure 9*b–d*, we added a differential equation for m_{T}:

$$\dot{m}_{\mathrm{T}} = \phi_{m_{\mathrm{T}}}\tau_{m_{\mathrm{T}}}^{-1}(v)(m_{\mathrm{T}_\infty}(v) - m_{\mathrm{T}}),$$

where $\phi_{m_{\mathrm{T}}} = 5$ and:

$$\tau_{m_{\mathrm{T}}} = m_{\mathrm{T}_\infty}(v)(1.7 + \exp(-(v + 26.8)/13.5)).$$

PHILOSOPHICAL TRANSACTIONS OF THE ROYAL SOCIETY B BIOLOGICAL SCIENCES

For the nRT model of figure 11 the equations and parameter values were as above except that $v_{sep} = 1.45\,\text{mV}$, $g_{NaP} = 6\,\text{mS cm}^{-2}$, $\sigma_{NaP} = -12\,\text{mV}$, $g_K = 25\,\text{mS cm}^{-2}$ and $g_{Na} = 20\,\text{mS cm}^{-2}$.

APPENDIX 4. EQUATIONS AND PARAMETER VALUES FOR THE MODIFIED WANG, RINZEL AND ROGAWSKI MODEL

The equations are:

$$\dot{v} = C^{-1}\{-I_T - I_K - I_L - I_{KCa(T)} + I_{Ext} + I(t)\},$$

$$\dot{m}_T = \tau_{m_T}^{-1}(v)(m_{T_\infty}(v) - m_T),$$

$$\dot{h} = \alpha_1(1 - h - d) - \beta_1 h,$$

$$\dot{d} = \beta_2(1 - h - d) - \alpha_2 h,$$

$$\dot{c} = -kI_T - k_{Ca}c,$$

where $C = 1\,\mu\text{F cm}^{-2}$ and $I_T = g_T m_T^3 h(v - v_{Ca})$, $I_K = g_K n_\infty^4(v - v_K)$, $I_L = g_L(v - v_L)$ and $I_{KCa(T)} = g_{KCa(T)}(c/K_{Ca(T)} + c)(v - v_K)$.

For I_K:

$$\alpha_n(v) = \frac{-0.096(v + 45 + \sigma_K)}{(\exp(-0.2(v + 45 + \sigma_K)) - 1)},$$

$$\beta_n(v) = 1.5\exp(-(v + 50 + \sigma_K)/40),$$

$$n_\infty(v) = \frac{\alpha_n(v)}{\alpha_n(v) + \beta_n(v)},$$

and $g_K = 5\,\text{mS cm}^{-2}$, $v_K = -105\,\text{mV}$, $\sigma_K = 15\,\text{mV}$.

For I_T:

$$m_{T_\infty}(v) = \frac{1}{1 + \exp\{-(v + v_M - \theta_{m_T})/7.8\}},$$

$$\tau_{m_T}(v) = 0.2 m_{T_\infty}(v) \times (1.7 + \exp\{-(v + v_M + 28.8)/13.5),$$

$$K = \sqrt{[0.25 + \exp\{(v + v_H - \theta_{h_T})/6.3\}]} - 0.5,$$

$$\alpha_1 = 3\exp\{-(v + v_H + 160.3)/17.8\},$$

$$\beta_1 = \alpha_1 K$$

$$\tau_2 = 0.33\frac{240}{1 + \exp\{(v + v_H + 37.4)/30\}},$$

$$\alpha_2 = \frac{1}{\tau_2(1 + K)},$$

$$\beta_2 = \alpha_2 K,$$

and $v_M = 2\,\text{mV}$, $v_H = -8.5\,\text{mV}$, $g_T = 1\,\text{mS cm}^{-2}$, $v_{Ca} = 120\,\text{mV}$, $\theta_{m_T} = -63\,\text{mV}$, $\theta_{h_T} = -83.5\,\text{mV}$.

For I_L:

$g_L = 0.1\,\text{mS cm}^{-2}$, $v_L = -65\,\text{mV}$.

For $I_{KCa(T)}$:

$g_{KCa(T)} = 1\,\text{mS cm}^{-2}$, $v_K = -105\,\text{mV}$, $k = 0.001\,\mu\text{M cm}^{-2}\,\mu\text{A}^{-1}\,\text{ms}^{-1}$, $k_{Ca} = 0.044\,\text{ms}^{-1}$, $K_{Ca(T)} = 1\,\mu\text{M}$.

The relevant values of I_{Ext} and $I(t)$ are given in the text and the figure legends.

REFERENCES

Avanzini, G., de Curtis, M., Panzica, F. & Spreafico, R. 1989 Intrinsic properties of nucleus reticularis thalami neurones of the rat studied *in vitro*. *J. Physiol., Lond.* **416**, 111–122.

Bal, T. & McCormick, D.A. 1993 Mechanisms of oscillatory activity in guinea-pig nucleus reticularis thalami *in vitro*: a mammalian pacemaker. *J. Physiol., Lond.* **468**, 669–691.

Blatz, A.L. & Magleby, K.L. 1987 Calcium-activated potassium channels. *Trends Neurosci.* **10**, 463–467.

Chay, T.R. & Keizer, J. 1983 Minimal model for membrane oscillations in the pancreatic β-cell. *Biophys. J.* **42**, 181–190.

Connor, J.A. & Stevens, C.F. 1971 Prediction of repetitive firing behaviour from voltage clamp data on an isolated neurone soma. *J. Physiol., Lond.* **213**, 31–53.

Coulter, D.A., Huguenard, J.R. & Prince, D.A. 1989 Calcium currents in rat thalamocortical relay neurones: kinetic properties of the transient low-threshold current. *J. Physiol., Lond.* **414**, 587–604.

Crunelli, V., Lightowler, S. & Pollard, C.E. 1989 A T-type Ca^{2+} current underlies low threshold Ca^{2+} potentials in cells of the cat and rat lateral geniculate nucleus. *J. Physiol., Lond.* **413**, 543–561.

Destexhe, A. & Babloyantz, A. 1993 A model of the inward current I_h and its possible role in thalamocortical oscillations. *NeuroReport* **4**, 223–226.

Destexhe, A., Babloyantz, A. & Sejnowski, T.J. 1993 Ionic mechanisms for intrinsic slow oscillations in thalamic relay neurons. *Biophys. J.* **65**, 1538–1552.

Destexhe, A., Lytton, W.W., Sejnowski, T.J., McCormick, D.A., Contreras, D. & Steriade, M. 1993 A model of 7–14 Hz spindling in the thalamus and thalamic reticular nucleus: interaction between intrinsic and network properties. *Soc. Neurosci. Abstracts* **19**. (In the press.)

Gutnick, M.J. & Yarom, Y. 1989 Low threshold calcium spikes, intrinsic neuronal oscillation and rhythm generation in the CNS. *J. Neurosci. Meth.* **28**, 93–99.

Hernández-Cruz, A. & Pape, H-C. 1989 Identification of two calcium currents in acutely dissociated neurons from the rat lateral geniculate nucleus. *J. Neurophysiol.* **61**, 1270–1283.

Hindmarsh, J.L. & Rose, R.M. 1992 A model for low threshold oscillations in neurons. In *Coupled oscillating neurons* (ed. J. G. Taylor & C. L. T. Mannion), pp. 81–97. London: Springer-Verlag.

Hindmarsh, J.L. & Rose, R.M. 1994*a* Resonance in a model of a mammalian neuron *Phil. Trans. R. Soc. Lond.* B **346**, 151–163. (Following paper.)

Hindmarsh, J.L. & Rose, R.M. 1994*b* A model of intrinsic and driven spindling in thalamocortical neurons. *Phil. Trans. R. Soc. Lond.* B **346**, 165–183. (This volume.)

Hodgkin, A.L. & Huxley, A.F. 1952 A quantitative description of membrane current and its application to conduction and excitation in nerve. *J. Physiol., Lond.* **213**, 31–53.

Huguenard, J.R., Coulter, D.A. & Prince, D.A. 1991 A fast transient potassium current in thalamic relay neurons: kinetics of activation and inactivation. *J. Neurophysiol.* **66**, 1304–1315.

Huguenard, J.R. & Prince, D.A. 1991 A slow inactivation of a TEA-sensitive K current in acutely isolated rat thalamic relay neurons. *J. Neurophysiol.* **66**, 1316–1328.

Jahnsen, H. & Llinás, R. 1984*a* Electrophysiological properties of guinea-pig thalamic neurons: an *in vitro* study. *J. Physiol., Lond.* **349**, 205–226.

Jahnsen, H. & Llinás, R. 1984*b* Ionic basis for the

PHILOSOPHICAL TRANSACTIONS OF THE ROYAL SOCIETY B BIOLOGICAL SCIENCES

electroresponsiveness and oscillatory properties of guinea-pig thalamic neurons *in vitro*. *J. Physiol.*, *Lond.* **349**, 227–247.

Leresche, N., Lightowler, S., Soltez, I., Jassik-Gerschenfeld, D. & Crunelli, V. 1991 Low frequency oscillatory activities intrinsic to rat and cat thalamocortical cells. *J. Physiol.*, *Lond.* **441**, 155–174.

Llinás, R. & Yarom, Y. 1986 Oscillatory properties of guinea-pig inferior olivary neurons and their pharmacological modulation: *in vitro* study. *J. Physiol.*, *Lond.* **376**, 163–182.

Lytton, W.W. & Sejnowski, T.J. 1992 Computer model of ethosuximide's on a thalamic cell. *Annls Neurol.* **32**, 131–139.

McCormick, D.A. & Pape, H.C. 1990 Properties of a hyperpolarization activated cation current and its role in rhythmic oscillation in thalamic relay neurons. *J. Physiol.*, *Lond.* **431**, 291–318.

Pennefather, P., Lancaster, B., Adams, P.R. & Nicoll, R.A. 1985 Two distinct Ca-dependent K currents in bullfrog sympathetic ganglion cells. *Proc. natn. Acad. Sci. U.S.A.* **82**, 3040–3044.

Plant, R.E. 1978 The effects of calcium^{++} on bursting neurons: a modelling study. *Biophys J.* **21**, 217–237.

Rinzel, J. & Lee, Y.S. 1986 On different mechanisms for membrane potential bursting. In *Nonlinear oscillations in biology and chemistry* (*Lecture notes in biomathematics* vol. 66) (ed. H. G. Othmer), pp. 19–33. New York: Springer.

Rose, R.M. & Hindmarsh, J.L. 1989*a* The assembly of ionic currents in a thalamic neuron. I. The three-dimensional model. *Proc. R. Soc. Lond.* B **237**, 267–288.

Rose, R.M. & Hindmarsh, J.L. 1989*b* The assembly of ionic currents in a thalamic neuron. II. The stability and state diagrams. *Proc. R. Soc. Lond.* B **237**, 289–312.

Rose, R.M. & Hindmarsh, J.L. 1989*c* The assembly of ionic currents in a thalamic neuron. III. The seven-dimensional model. *Proc. R. Soc. Lond.* B **237,** 313–334.

Soltez, I., Lightowler, S., Leresche, N., Jassik-Gerschenfeld, D., Pollard, C.E. & Crunelli, V. 1991 Two inward currents and the transformation of low frequency oscillations of rat and cat thalamocortical cells. *J. Physiol.*, *Lond.* **441**, 175–197.

Tasker, J.G. & Dudek, F.E. 1991 Electrophysiological properties of neurones in the region of the paraventricular nucleus in slices of rat hypothalamus. *J. Physiol.*, *Lond.* **434**, 271–293.

Toth, T. & Crunelli, V. 1992 Computer simulations of the pacemaker oscillations of thalamocortical cells. *NeuroReport* **3**, 65–68.

von Krosigk, M., Bal, T. & McCormick, D.A. 1993 Cellular mechanisms of a synchronized oscillation in the thalamus. *Science*, *Wash.* **261**, 361–364.

Wang, X.-J. 1994 Multiple dynamical modes of thalamic relay neurons: rhythmic bursting and intermittant phase-locking. *Neuroscience* **59**, 21–31.

Wang, X.-J. & Rinzel, J. 1993 Spindle rhythmicity in the reticularis thalami nucleus: synchronization among mutually inhibitory neurons. *Neuroscience* **53**, 899–904.

Wang, X.-J., Rinzel, J. & Rogawski, M.A. 1991 A model of the T-type calcium current and the low-threshold spike in thalamic neurons. *J. Neurophysiol.* **66**, 839–850.

Wilcox, K.S., Gutnick, M.J. & Christoph, G.R. 1988 Electrophysiological properties of neurons in the lateral habenula nucleus: an *in vitro* study. *J. Neurophysiol.* **59**, 212–225.

Yarom, Y. 1991 Rhythmogenesis in a hybrid system – interconnecting an olivary neuron to an analog network of coupled oscillators. *Neuroscience* **44**, 263–275.

Received 3 February 1994; accepted 3 May 1994

PHILOSOPHICAL TRANSACTIONS OF THE ROYAL SOCIETY B BIOLOGICAL SCIENCES